COMBINED DEM-FEM MODELING OF SHOT PEENING PROCESS

by

Dhanooj Bobba

A thesis submitted to the faculty of
The University of North Carolina at Charlotte
in partial fulfillment of the requirements
for the degree of Master of Science in
Mechanical Engineering

Charlotte

2018

Approved by:

_____

Dr. Harish P. Cherukuri

_____

Dr. Praveen Ramaprabhu

_____

Dr. Vincent Ogunro

ABSTRACT

DHANOOJ BOBBA. Combined DEM-FEM Modeling of Shot Peening Process.
(Under the direction of DR. HARISH P. CHERUKURI)

Shot peening is a commonly used technique for improving the fatigue life of machine components by inducing compressive residual stresses in the surface layers. This process involves plastically deforming the surface layers by impacting the surfaces with spherical particles at high speeds. The induced residual compressive stresses resist crack propagation and thus increase the fatigue life. The intensity of shot peening, measured using the Almen test, is an essential quantity for ensuring shot peening effectiveness and repeatability. It depends on various process parameters such as the shot speed, shot size, shot material, impact direction, and flow rate. Therefore, a thorough understanding of the impact of these parameters on shot peening intensity is critical for analyzing and optimizing the process.

In this thesis work, a novel computational model is developed to accurately simulate the Almen intensity tests on a Type-C strip. The model uses a coupled technique based on the discrete element method (DEM) and the conventional finite element method (FEM). The shots are generated randomly and their motion is analyzed using DEM. The interaction of the shots with the Almen strip and the deformation of the Almen strip are analyzed using FEM. The shots, spherical in shape, are treated as rigid particles while the mechanical response of the Almen strip is modeled using the Johnson-Cook constitutive model. The predicted Almen intensity values agree with analytically calculated values and are found to be within the experimentally reported range of values for Almen intensities. Results from the parametric studies conducted to analyze the influence of shot speed, impact direction and shot sizes on the Almen intensity indicate that a given Almen intensity can be obtained by many different combinations of these parameters although the residual stress fields may be different.

An important conclusion from this observation is that similar Almen intensities do not necessarily mean similar values for fatigue life.

ACKNOWLEDGEMENTS

I would like to thank my academic advisor Dr. Harish Cherukuri for his continuous support, guidance and mentoring me throughout my Master's degree program. And also I would like to thank Dr. Praveen Ramaprabhu for giving us access to his senior design project and Dr. Vincent Ogunro for being a part of this committee. I would also like to thank my family, friends and colleagues for their support and making my stay at UNCC memorable.

TABLE OF CONTENTS

LIST OF FIGURES viii

LIST OF TABLES xi

CHAPTER 1: INTRODUCTION 1

1.1. Coverage Area 3

1.2. Almen Intensity 4

CHAPTER 2: LITERATURE REVIEW 7

CHAPTER 3: DISCRETE ELEMENT METHOD 13

CHAPTER 4: NUMERICAL MODEL 17

4.1. Geometry 17

4.2. Constitutive Model 20

4.3. Analysis 22

4.4. Contact Algorithm 26

4.5. Boundary and Initial Conditions 29

4.6. Element Type and Meshing 32

CHAPTER 5: RESULTS AND VERIFICATION 35

5.1. Results 35

5.2. Verification 44

CHAPTER 6: PARAMETRIC STUDY 48

6.1. Shot Velocity 48

6.2. Angle of Impact 51

6.3. Shot size 55

6.4. Almen intensity 59

CHAPTER 7: CONCLUSIONS 63

REFERENCES 66

LIST OF FIGURES

FIGURE 1.1: Compressive residual stresses due to shot peening. 2

FIGURE 1.2: Effect of peening passes on coverage area. [8] 3

FIGURE 1.3: Almen strip test. [9] 4

FIGURE 1.4: Saturation curve. 5

FIGURE 3.1: Shortened figure caption for list of figures. 14

FIGURE 3.2: A schematic of DEM calculations. [35] 15

FIGURE 4.1: Type-C Almen strip. 18

FIGURE 4.2: Almen strip with a supporting rigid plate. 19

FIGURE 4.3: Particle generator with DEM shots. 19

FIGURE 4.4: Stress vs. Equivalent plastic strain for varying strain-rates. 22

FIGURE 4.5: Contact between the DEM particles and the Almen strip. 27

FIGURE 4.6: The highlighted areas are fully constrained to represent the action of the bolts on the strip. 29

FIGURE 4.7: The particle generator is constrained to move in only the x direction. 30

FIGURE 4.8: Mesh. 33

FIGURE 4.9: Biased mesh. 33

FIGURE 5.1: Deflection of Almen strip (isometric view). 36

FIGURE 5.2: Deflection of Almen strip (side view). 36

FIGURE 5.3: Normal stress distribution (S_{11}) in the top surface (constrained state). 37

FIGURE 5.4: Normal stress distribution (S_{11}) in the top surface (unconstrained strip). 37

FIGURE 5.5: Normal stress distribution (S_{11}) in the bottom surface (constrained state). 38

FIGURE 5.6: Normal stress distribution (S_{11}) in the bottom surface (unconstrained strip). 38

FIGURE 5.7: Stress (S_{11}) redistribution during the springback analysis. 39

FIGURE 5.8: Saturation curve. 40

FIGURE 5.9: Effect of number of peening passes on the stresses in the constrained strip. 42

FIGURE 5.10: Effect of number of peening passes on the stresses in the unconstrained strip. 42

FIGURE 5.11: Effect of number of peening passes on equivalent plastic strains (constrained). 43

FIGURE 5.12: Effect of number of peening passes on equivalent plastic strains (unconstrained). 43

FIGURE 6.1: Effect of impact velocity on the Almen intensity. 49

FIGURE 6.2: Effect of impact velocity on the induced stresses in constrained strip. 49

FIGURE 6.3: Effect of impact velocity on the residual stresses in unconstrained strip. 50

FIGURE 6.4: Effect of impact velocity on the equivalent plastic strains. 50

FIGURE 6.5: Equivalent plastic strains in a cross section vs velocity (a) 80 m/s, (b) 70 m/s & (c) 60 m/s. 51

FIGURE 6.6: Maximum equivalent plastic strains vs. impact velocities. 52

FIGURE 6.7: Effect of angle of impact on Almen intensity. 52

FIGURE 6.8: Effect of angle of impact on the induced stresses in constrained strip. 53

FIGURE 6.9: Effect of angle of impact on the residual stresses in unconstrained strip. 53

FIGURE 6.10: Effect of angle of impact on the equivalent plastic strains. 54

FIGURE 6.11: Equivalent plastic strains in a cross section vs impact angles (a) 90^o, (b) 75^o & (c) 60^o . 54

FIGURE 6.12: Maximum equivalent plastic strains vs. impact angles. 55

FIGURE 6.13: Effect of shot size on Almen intensity. 56

FIGURE 6.14: Effect of shot size on the induced stresses in constrained strip. 57

FIGURE 6.15: Effect of shot size on the residual stresses in unconstrained strip. 57

FIGURE 6.16: Effect of shot size on the equivalent plastic strains. 58

FIGURE 6.17: Equivalent plastic strains in a cross section vs shot size (a) 0.2 mm, (b) 0.15 mm & (c) 0.1 mm . 58

FIGURE 6.18: Maximum equivalent plastic strains vs. shot size. 59

FIGURE 6.19: Induced stresses in a constrained strip. 60

FIGURE 6.20: Residual stresses in an unconstrained strip. 61

FIGURE 6.21: Equivalent plastic strains. 61

FIGURE 6.22: Equivalent plastic strains in a cross section (a) Velocity-70m/s, (b) Shot size-0.15mm & (c) Impact Angle-60^o . 62

LIST OF TABLES

TABLE 4.1: Chemical composition of SAE 1070 Steel[9]. 20

TABLE 4.2: Mechanical properties of SAE 1070 Steel[9]. 21

TABLE 4.3: Johnson-Cook material constants for SAE 1070 Steel[9]. 21

TABLE 4.4: Amplitude function for displacements of particle generator. 30

TABLE 4.5: Amplitude function for initial velocity. 31

TABLE 4.6: Amplitude function for mass flow rate. 31

TABLE 5.1: Comparison of simulated Almen intensities with analytical model. 47

TABLE 6.1: Combinations of peening parameters for same Almen intensity. 59

CHAPTER 1: INTRODUCTION

Propagation of surface cracks is one of the leading causes of the failure of machine components. Many metal working procedures such as milling, grinding and bending induce tensile residual stresses which promote crack propagation and thus, decrease the fatigue life of the components [1]. And in industries, as most of the machine parts are regularly subjected to alternating loads, the presence of these tensile residual stresses will require a regular replacement the components while driving up the maintenance costs. As a result, to remove these unnecessary tensile residual stresses, the components are subjected to special purpose techniques commonly known as work hardening or surface hardening techniques. These procedures involve hardening of the surface of a metallic component by inducing compressive residual stresses which resist the propagation of cracks and thereby increasing the fatigue life of the machine components [2, 3].

Work hardening or surface hardening is a long-established process of strengthening of metals by inducing compressive residual stresses or relieving tensile stresses already present in the workpiece through plastic deformations. In fact, surface hardening of metals has been dated back to 2700 BC [4], where the metallic surfaces were indented with blunt objects to induce compressive residual stresses. Using a similar concept of inducing compressive residual stresses by indentation, shot peening was first developed in early 1930s, and it has been extensively used in early 1940s to improve the fatigue life of critical aircraft components during the second world war [5]. By 1950, the realization of the benefits of shot peening machine components lead to its wide-ranging applications in aerospace, energy generation, and automobile industries.

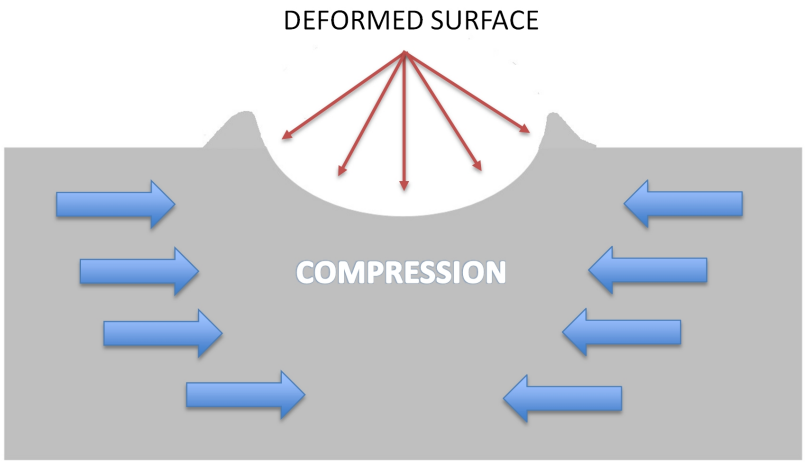

Figure 1.1: Compressive residual stresses due to shot peening.

Shot peening is a complex cold working process used to improve the fatigue life of the metallic components. In this process, the surface of the components is indented with a large number of small spherical shots with high velocities. These indentations result in localized plastic deformations at the site of the impact. The subsequent elastic recovery of these deformations leads to the development of compressive residual stresses in the surface [6], as shown in Figure 1.1. These residual stresses prevent the propagation of cracks from the surface, thereby increasing the fatigue life of the shot peened components. The commonly used shot media are spherical cast steel, ceramic shots, glass beads or conditioned cut wire.

Effectiveness and repeatability of the shot peening process are determined mainly by two factors, coverage area, and peening intensity. Coverage area is defined as the percentage of the surface of a component that has been indented at least once by the peening media. The peening intensity corresponds to the amount of energy transferred from a shot to the workpiece during the impact, and it is related to the kinetic energy of the shot stream [7]. These two factors, in turn, depend on various shot peening parameters such as shot velocity, shot size, shot material properties, target material properties, impact angle, the distance of the nozzle from the specimen. A comprehensive analysis of the impact of these parameters on the intensity and the

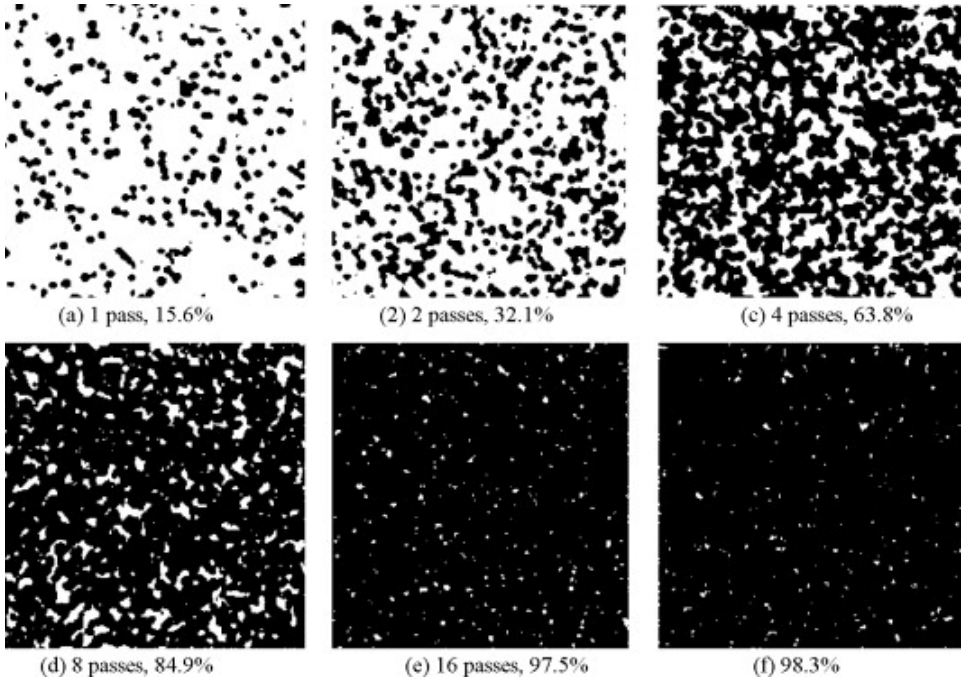

Figure 1.2: Effect of peening passes on coverage area. [8]

coverage area is crucial in evaluating the development of the residual stress state and in the overall optimization of the shot peening process.

1.1 Coverage Area

Coverage area is defined as the percentage of the surface of a workpiece that has been indented at least once by the shot media. In other words, it is the ratio of peened area to the total area of the workpiece. As shown in Figure 1.2, the percentage of indented area increases with increase in the number of nozzle passes over the workpiece, which is analogous to the peening time. And it can be observed that as the peening time increases, the new indents overlapping with a previous indents increases, without making any contribution to the coverage. As a result, it is very difficult to obtain an accurate measurement of coverage above 98%. Hence coverage of approximately around 98% is defined as the full coverage. And to obtain coverage above full coverage, the peening time is increased in the multiples of time required for full coverage, i.e., if full coverage is obtained at time T, then to obtain a coverage

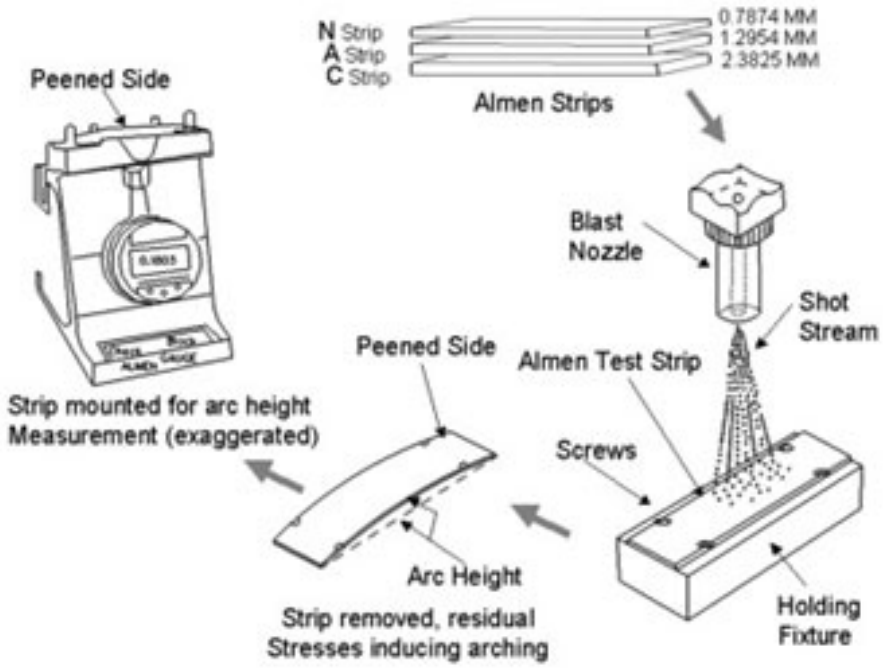

Figure 1.3: Almen strip test. [9]

of around 200% the peening time is increased to $2T$.

During shot peening process, achieving full coverage ensures the uniform distribution of compressive residual stresses which are essential for the increase in fatigue life of the components. On the other hand, over-peening or excessive coverage leads to a large number of overlap of impacts which will lead to damage to the material being peened. Hence measurement of coverage area is essential for the determination of the quality of the peening process. The commonly used techniques to measure coverage are visual inspection using magnification, scanning electron microscopy and blue dye or fluorescent coating procedures.

1.2 Almen Intensity

The intensity of the peening process is defined as the average dent capability of an individual shot particle in a shot stream. It is related to the energy of the shot stream. It is measured in terms of the radius of curvature of a thin metallic strip due to shot peening. Almen and Black [7] proposed an indirect method to measure the

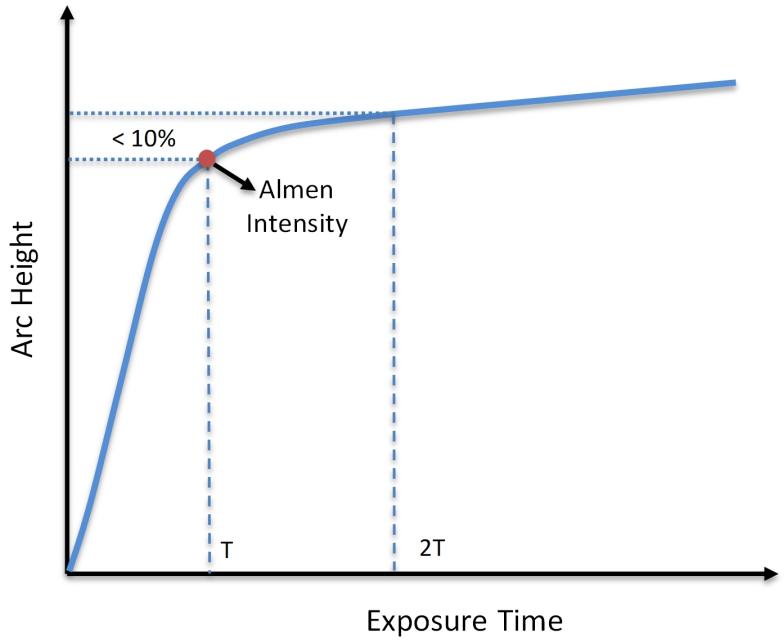

Figure 1.4: Saturation curve.

intensity of the peening process. They shot peened a thin metallic strip, also known as Almen strips, by fixing them onto a holder with the help of four bolts, as shown in Figure 1.3. When these bolts are removed after the shot peening process, the strip bends in the direction of peening forming an arc. A special gauge, commonly known as the Almen gauge, is used to measure the height at the center of the arc. These arc-heights are used to measure the intensity of the peening process. The saturation curve or Almen intensity curve, shown in Figure 1.4, is obtained by plotting the measured arc-heights of the Almen strip, against their respective peening times. If the arc-height at a certain peening time T increases less than 10% when the peening time is doubled, i.e., $2T$, then the arc-height at time T on the saturation curve is known as the Almen intensity.

The intensity of the peening process depends on many process parameters such as shot size, impact velocity, the angle of impact, etc. And the measurement of each of these individual parameters is a laborious task as shot peening involves a large of particles which are difficult to track individually. Hence Almen intensity is used as an

indirect measure to ensure the consistency and repeatability of the peening process. It is essential to have a clear understanding of these control parameters to analyze and optimize the process. Hence in this study, a numerical model has been developed to simulate the shot peening process on the Almen strips. The effect of process parameters such as shot velocity, shot size and angle of impact on the intensities have been analyzed.

CHAPTER 2: LITERATURE REVIEW

The ability of the shot peening process to induce compressive residual stresses and extend the fatigue life of many components led to its extensive use as a valuable surface treatment process in many different industries. This led to an immense interest in understanding the theoretical aspects of shot peening to analyze and optimize the overall process. As a result, few experimental studies have been done to study the influence of various parameters on the shot peening process. Cao et al. [10] studied the effect of impact velocities under different shot sizes on the development of the arc-height. They investigated the residual stresses in a Type-A Almen strip both in constrained state and free state for different peening times, using surface profilometry and X-ray diffraction. Miao et al. [8] studied the influence of shot velocity and peening time on intensity, coverage and surface roughness in aluminum strips using ceramic shots. However, the experimental analysis of shot peening process is complicated as well as expensive. And also the experimental measurement of stresses induced in the workpiece after shot peening is very expensive and often uses destructive methods such as X-ray diffraction. These complications with the experimental procedures along with the steadily increasing computational power led to the development of analytical and numerical models which were used to study the impact of various process parameters and to predict the stress state developed due to shot peening process.

Few analytical models of shot peening have been developed over the past few decades, using the fundamental quasi-static approaches of Hertz contact theory [11]. Li et al. [12] developed an analytical model to calculate the compressive residual stresses considering only the impact of a single shot. Guagliano [13] developed a

model to estimate the Almen arc height using the residual stresses imparted to the workpiece during shot peening. He used this model to relate the arc-height with the shot peening velocity for different shot sizes. Miao et al. [14] proposed a combined model to predict the residual stresses and deformed arc height in the Almen strip. They investigated the influence of shot peening parameters such as shot velocity and shot size on the Almen intensity and the residual stresses. Guechichi et al. [15] used a similar model for predicting the impact velocities from the arc-heights of the Almen strips. Even though some of these analytical models were able to closely predict the residual stress state and arc-heights of Almen strips after the shot peening process, numerical models provide much more comprehensive analysis of stress development with multiple shots while considering the complex material deformations of the specimen.

The early computational studies considered axisymmetric models to simulate a single shot impact on cylindrical or semi-infinite bodies [16]. Follansbee et al. [17] and Sinclair et al. [18] used an axisymmetric model with the quasi-static approach to study the stress state in an elasto-plastic material due to normal indentation. Mori et al. [19] used a similar model to study the effects of shot deformation behavior on the residual stress state. They also considered friction in the model and determined that it is an influencing parameter on the residual stress state. Schiffner et al. [20] developed an axisymmetric model to analyze the residual stress profiles and indentation depth in an elasto-plastic surface with different shot-peening parameters. But the inability of these models to simulate inclined impacts and multiple shot impacts with the corresponding coverage effects lead to the development of three-dimensional finite element models.

Three-dimensional shot peening models have been used to study the effects of a single shot with an inclined angle of impact or multiple shots impacts on the stresses developed due to shot peening. Hong et al. [21] studied the effects of a single shot on

a semi-circular plate with symmetric boundary conditions. They studied the effects of impact angle, material parameters and strain hardening parameter along with the shot diameter on the residual stress state. Al-Obaid [22] used a quarter plate model with three-dimensional isoparametric finite elements to analyze the residual stresses developed due to shot peening. He studied the mechanics of single shot indentation due to both static and dynamic loading. Meguid et al. [23] used a similar model to study the time history of shot velocity and contact forces during the shot indentation. They also analyzed the impact of shot size, shot shape and the target material hardening characteristics on the depth of the compressed layer developed due to shot peening. Shivpuri et al. [24] modeled a 3D circular plate with symmetric boundary conditions to study the effects of coefficient of friction and multiple impacts on the magnitude of the compressive residual stresses and the depth of indentation. As mentioned above these models have been used to study the effects of single shot or multiple shot impacts at the same location on the residual stress state, but in the shot peening process, the developed residual stress state is dependent on the shots impacting at multiple locations on the target. As a result, various finite element models have been developed to study the effect the shots impacting at various locations. Meguid et al. [25] considered layers of shots, impacting the target and developed a symmetric model with four uniformly spaced shot impacts, with each shot representing a different row. They studied the effects of strain rate, shot deformation, peening coverage and friction on the residual stresses developed due to shot peening. Majzoobi et al. [26] developed a similar model with Johnson-Cook material parameters to account for the stress wave propagation, strain and strain rate hardening. They compared the numerical model with a single shot experiment and found a reasonable agreement between the results. They used this numerical model to study the effects of a different arrangement of shots on the residual stresses.

In the models mentioned above, contrary to the actual shot peening process the

shot sequence and impact locations were defined as a priory. And they cannot be used to study the shot peening intensity and coverage as they were limited to a very few number of shots. Miao et al. [27] developed a three-dimensional finite element model with randomly distributed shot over an aluminum plate. They studied the effect of a different number of shots (upto 96) and angle of incidence on the intensity, coverage and surface roughness. They found that in case of oblique impact, the full coverage was achieved much faster than the normal impact. Kang et al. [28] used a similar model with a special series of impacts to create a uniformly distributed shot over the target. They analyzed the development of plastic strains, residual stresses and the subsequent deflection of the target using springback analysis. Bhuvaraghan et al. [9] modeled a random distribution of shot over a thin slice of an Almen strip to analyze the effects of shot size and velocity on the intensity. They analyzed the compressive residual stress state developed due to shot peening in two different target materials. Chen et al. [29] developed a similar model with a random distribution of shot to simulate the Almen intensity tests. They modeled a quarter of the Almen strip with symmetric boundary conditions to study the effect of shot velocity on the Almen intensity. They analyzed the stresses developed in an Almen strip for different shot peening parameters. Although the finite element models were able to closely simulate the shot peening process, the involvement of a large number of particles in the process made it difficult to develop a full scale model using only finite elements. To cut the computational cost of the models, many researchers used reduced models with simplified boundary conditions along with a limited number of shots.

Particle dynamic models have gained the interest of the shot peening community in recent years, for their ability to model the particulate flows [16]. They have been used to model the shot stream to analyze the various aspects of shot dynamics during the shot peening process. Hong et al. [21] used discrete element method to model the shot stream and studied the effects of the number of shots, initial velocity, the angle of

attack and shot diameter on the impact velocity of the shot stream. Bhuvaraghan et al. [30] transferred the contact location and forces obtained from the discrete element method to FEM and analyzed the residual stress state. They assumed the coefficient of restitution to be constant in the model. Murugaratnam et al. [31] used a similar model by varying the coefficient of restitution depending on the number of impacts at the same location. They studied the effect of various process parameters on the shot stream dynamics and final velocities. Jebahi et al. [32] used coupled DEM-FEM model with representative element volumes to reduce the computational cost of the model. Although these models were able to simulate a large number of shots, they were limited to the study of shot stream dynamics. Few researchers developed combined DEM-FEM models to analyze the residual stresses, but in these models the coefficient of restitution has been defined as a constant or as a function of the number of impacts, ignoring the effect of other parameters involved in the process.

Considering the limitations of the previous models, in this study, a coupled DEM-FEM model has been used to simulate the shot peening of Almen strips. The shots are modeled using the DEM capabilities of Abaqus\2017 and the finite elements have been used to model the Almen strip. Contrary to the similar models used in literature, the coefficient of restitution is calculated as an internal variable depending on the specified process parameters. To verify the model, simulated results are compared to the experimental analysis from the literature. Using this model, effect of shot size, shot velocity and angle of impact on the arc-height and the residual stress states have been analyzed.

The outline of the thesis is structured as follows: Following the literature review, chapter 3 presents an introduction to the discrete element method and discusses the advantages and limitations of the technique over the finite element method. In chapter 4, the geometry of the numerical model along with the material constitutive model and the boundary conditions have been discussed. This chapter also discusses the

types of analyses used for different parts of the simulation. In chapter 5, the results from the springback analysis are analyzed and also the verification of the model has been carried out by comparing the obtained results with the analytical model. The effect of shot size, velocity, and angle of impact on the intensity and residual stresses have been discussed in chapter 6. Finally, in chapter 7, conclusions are drawn from the obtained results.

CHAPTER 3: DISCRETE ELEMENT METHOD

Discrete element method (DEM) is a particle based technique that is extensively used to model particulate or granular materials. It is a transient analysis that considers the dynamic interactions of a system of rigid particle. In this method, the contacting particles are connected by virtual rigid spring damper systems that simulate the contact interactions. As the particles move away from each other the contacts are broken and the springs are removed and at the same time when new contacts are formed additional springs are added into the system. The contact force acting on these particles is determined in two stages, commonly known as contact detection and contact resolution. In the detection stage, the particles that are in contact are identified and in the next step, the contact forces acting on each particles are calculated depending upon the defined contact constitutive model.

The contact models that are used in DEM can be divided into two groups known as soft sphere models and hard sphere models [33]. In hard sphere techniques, deformation or penetration is not allowed between the contacting particles, as shown in Figure 3.1(a). These models are based on the equations governing momentum exchange and the loss of the momentum during contact is defined through the coefficient of elastic restitution. In hard sphere models the events are analyzed sequentially, that is at most only one collision is allowed at any time during the simulation. Contrary to the preceding approach, in soft sphere techniques the particles are allowed to overlap at the site of the contact, as shown in figure 3.1(b). This approach is based on the equations governing linear and angular dynamic equilibrium of the colliding particles. And in contrast to the hard sphere techniques, soft sphere approach can simulate models with multiple simultaneous contacts, which led to its wider application for modeling

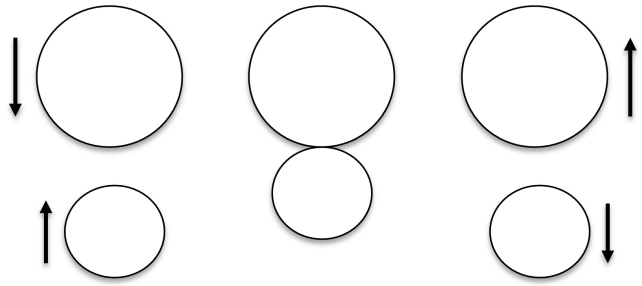

(a) Hard sphere technique.

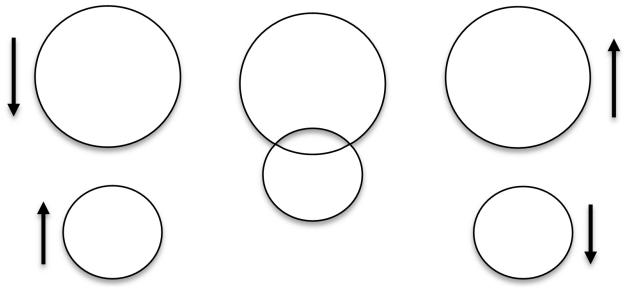

(b) Soft sphere technique.

Figure 3.1: Hard sphere and soft sphere approaches to DEM.

the granular material.

The basic formulation of the discrete element method was proposed by Cundall and Starck [34]. An overview of the steps involved in a DEM simulation is given in Figure 3.2 [35]. Initially the geometry of the system and the boundary conditions are defined by the user along with the appropriate contact model parameters. Then the simulation advances as a dynamic analysis for a given number of time increments. At each time step the contact between the particles is identified and the magnitude of the inter-particle forces is calculated. Then the dynamic equilibrium equations are solved to obtain the resultant forces and moments or torques on each particle. Using the particle inertia, the translational and rotational accelerations are calculated. The incremental displacements and rotations that are calculated in the current time step are used to update the particle positions and orientations in the next time step. Using these updated locations, the new contacts between the particles are identified and sequence of calculations are repeated.

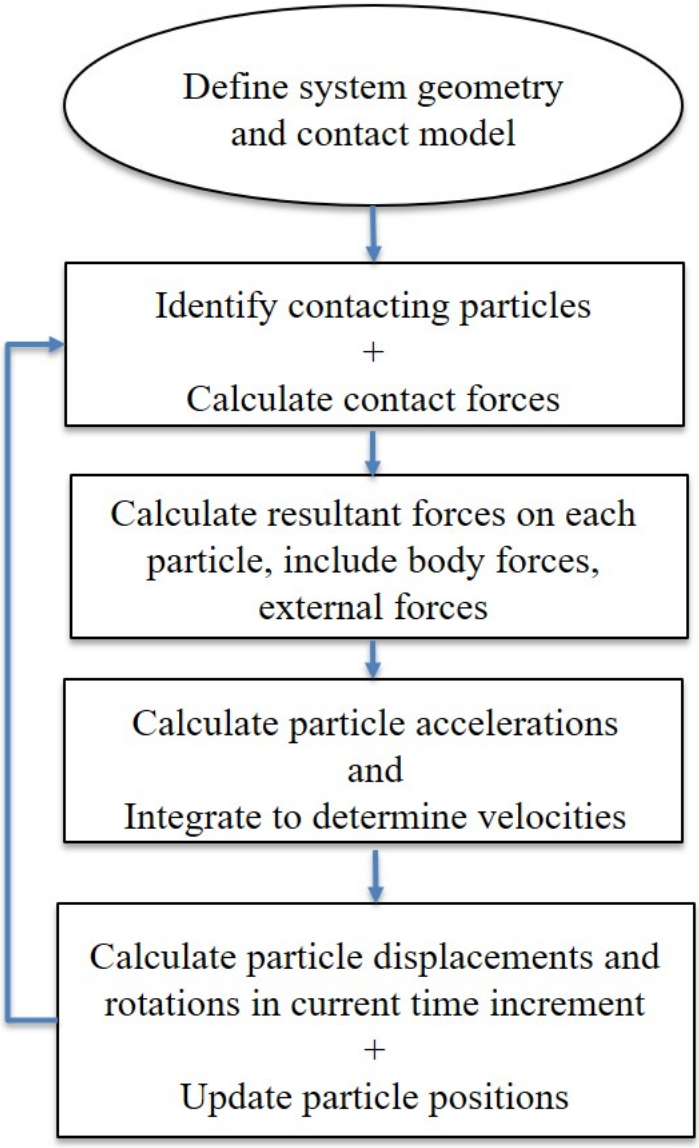

Figure 3.2: A schematic of DEM calculations. [35]

Discrete element method is used as an alternative for the continuum based techniques to model the granular material. In DEM, contrary to the continuum methods, the motion of the individual particles along with their interactions are explicitly considered. Along with that, DEM uses simplified particle shapes with basic models of contact, reducing the computational cost of the model. And analyzing large number of particles using DEM is relatively easy when compared to other continuum techniques. The main advantages for using this method is that, in DEM the particle scale mechanisms such as contact forces, particle orientations and rotations can be easily measured. And it is fairly simple to model large displacements in DEM when compared to the continuum based techniques such as finite element method. However, DEM uses an explicit time integration approach which requires a large number of small time increments in the simulation. And the need to include large number of particles in the simulation makes DEM computationally intensive. And also one of the main drawbacks of DEM is that the results are generated in terms of displacements and contact forces of individual particles, rather than in terms stresses and strains which have more physical meaning.

Considering the above mentioned advantages and limitations, in this thesis, a combined DEM-FEM model has been used to simulate the shot peening process. As shot peening involves a large number of particles which undergo large displacements, DEM has been used to model the shot stream. And the target has been modeled using the finite elements to analyze the residual stresses developed due to shot peening. A contact model has been defined between the DEM particles and the target in Abaqus\2017.

CHAPTER 4: NUMERICAL MODEL

The numerical model described in this chapter uses the combination of discrete element method and finite element method to simulate the shot peening process on Almen strips. The shots are modeled as a 3D rigid spheres using the discrete elements, and the strip is modeled as a rectangular block using the finite elements. Johnson-Cook constitutive model with strain-rate sensitivity is used to model the elasto-plastic characteristics of the Almen strip made of SAE 1070. The commercial finite element software package Abaqus is used in this study. The DEM capabilities of Abaqus\2017 are used to model the contact between the shots and the target. To reduce the complexity of the simulation shot-shot interactions are neglected in this study. The simulations are carried out in two steps, initially the shot peening process on the Almen strip is simulated using Abaqus\Explicit and the obtained results are then transferred to Abaqus\Standard to simulate the springback analysis. These simulations are run on Copperhead cluster (HPC) at University of North Carolina at Charlotte (UNCC). A typical run took about 20h on eight processors with 8GB ram each.

4.1 Geometry

A Type-C Almen strip with dimensions 76.2 mm $\times$ 18.9 mm $\times$ 2.39 mm is modeled as a thin rectangular block, as shown in figure 4.1. To simulate the actual shot peening process, the test strips are placed over a thin rectangular rigid plate, as shown in the figure 4.2, and a contact condition is defined. And a small rectangular plate with dimensions 7.62 mm $\times$ 18.9 mm, as shown in figure 4.3, is defined as a particle generator in Abaqus\Explicit to generate the DEM particles or shots in the

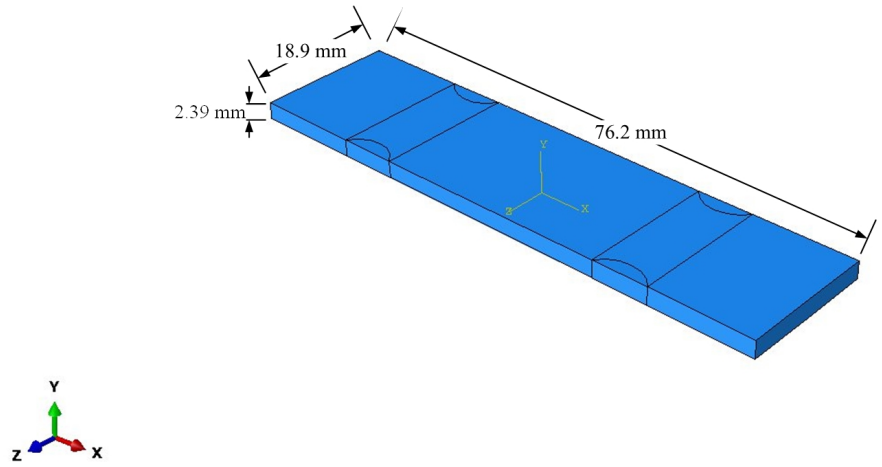

Figure 4.1: Type-C Almen strip.

simulation continuously. The top surface of the particle generator is defined as an inlet to inject the shots into the model. The maximum number of shots that can be used in the analysis is specified at the inlet as a priory. In Abaqus, the DEM particle sizes are determined by using statistical distributions [36]. These distributions can be defined by an analytical or user-defined linear tabular probability density functions. In this model, a discrete probability density function is defined which is given by the equation 4.1.

$$f_n = \begin{cases} x_1 & p_1 \\ x_2 & p_2 \\ .. & .. \\ x_n & p_n \end{cases} \tag{4.1}$$

where $x_1, x_2, ..., x_n$ are the desired sizes and $p_1, p_2, ..., p_n$ are the corresponding probabilities. In this study the shot size is assumed to be constant, so a single particle size with a probability distribution of one is defined.

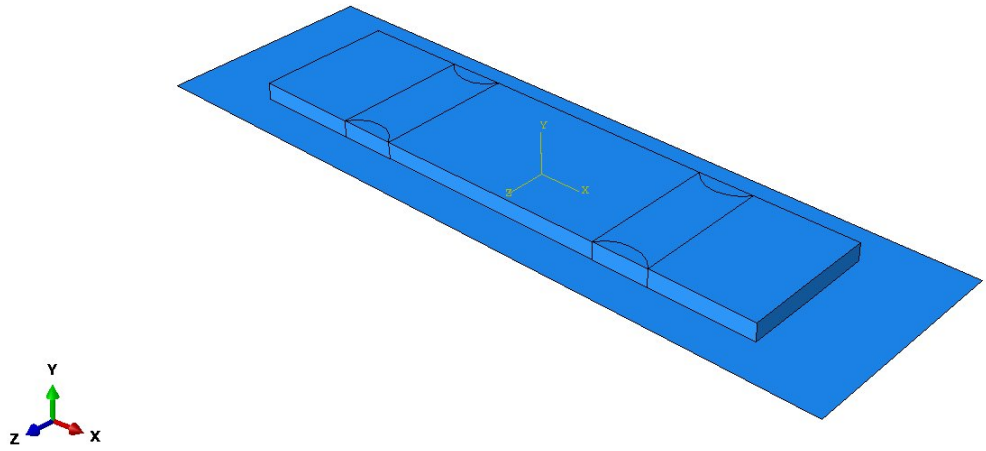

Figure 4.2: Almen strip with a supporting rigid plate.

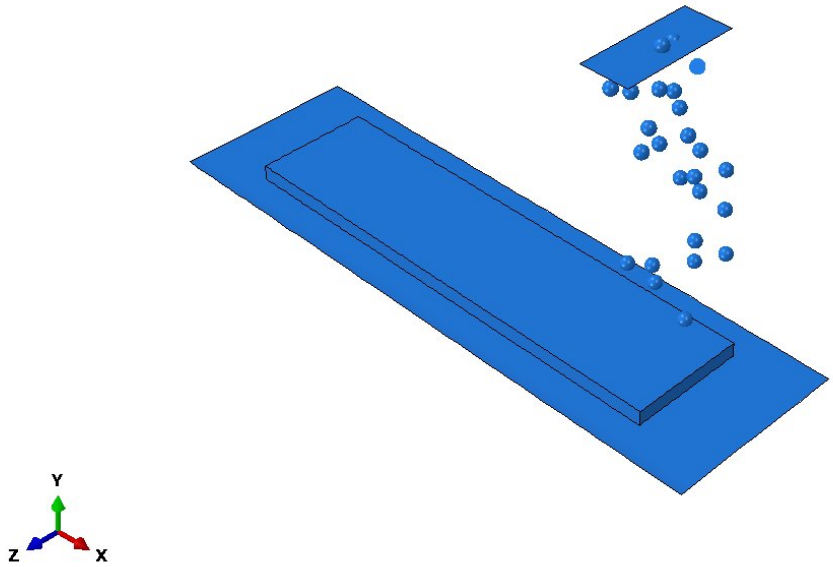

Figure 4.3: Particle generator with DEM shots.

4.2 Constitutive Model

The chemical composition of the Almen strips made of SAE 1070 steel is given in table 4.1. The mechanical properties are given in table 4.2. As shot peening involves very high strain rates [9], rate-dependent material properties should be used. And based on the literature, isotropic hardening model along with the rate-dependent properties is found to provide better stress distribution. Hence a Johnson-Cook material model, given by equation 4.2, is used in this study.

$$\sigma = [A + B\ \epsilon^n]\left[1 + C\ ln\ \dot{\epsilon^*}\right]\left[1 - T^{*^m}\right] \tag{4.2}$$

Here, σ is the flow stress which is a function of equivalent plastic strain ϵ, dimensionless plastic strain rate $\dot{\epsilon}^*$ which is given as shown in equation 4.3

$$\dot{\epsilon}^* = \frac{\dot{\epsilon}}{\dot{\epsilon}_o} \tag{4.3}$$

where $\dot{\epsilon}$ is the plastic strain rate and $\dot{\epsilon}_o$ is the reference plastic strain rate which is taken to be equal to one in this study. And T^{*^m} is the homogeneous temperature which is given by equation 4.4

$$T^{*^m} = \frac{(T - T_{ref})}{(T_m - T_{ref})} \tag{4.4}$$

where T_m is the melting temperature of the material and T_{ref} is the reference temperature or the room temperature. And A, B, C, n and m are the material constants, given in table 4.3.

Table 4.1: Chemical composition of SAE 1070 Steel[9].

Material	Composition (wt%)				
	C	Mn	S	P	Fe
SAE-1070	0.65-0.75	0.60-0.90	0.05(max)	0.04(max)	≈ 98

Table 4.2: Mechanical properties of SAE 1070 Steel[9].

Property	Value
Young's modulus (GPa)	200
Poission's ratio	0.3
Hardness (HRC)	44-50
Yield strength (MPa)	1268
Ultimate strength (MPa)	1422
% Elongation	8.2
Density (kg/m^3)	7800

Table 4.3: Johnson-Cook material constants for SAE 1070 Steel[9].

A (MPa)	B (MPa)	C	n	m
1408	600.8	0.0134	0.234	1

The Johnson-Cook's model calculates the stresses as a product of three different terms as shown in equation 4.2. The first term, $[A+B\epsilon^n]$ denotes the strain hardening of the material. Here A denotes the initial yield stress at room temperature, B is the coefficient of strain hardening, and n denotes the strain hardening exponent. And the second term $[1+Cln\dot{\epsilon}^*]$ is responsible for capturing the strain rate dependencies of the material where C represents the coefficient of strain rate hardening. Finally, the last term, $[1-T^{*^m}]$ represents the thermal softening and m denotes the thermal softening exponent. In this study, the thermal dependencies of the material are neglected. The stress vs. strain values for strain rates varying up to 10^5 are given in Figure 4.4.

The shots are modeled as a rigid particles in DEM with density 7850 kg/m^3, Young's modulus 200 GPa and Poission's ratio 0.25. Apart from these, a small

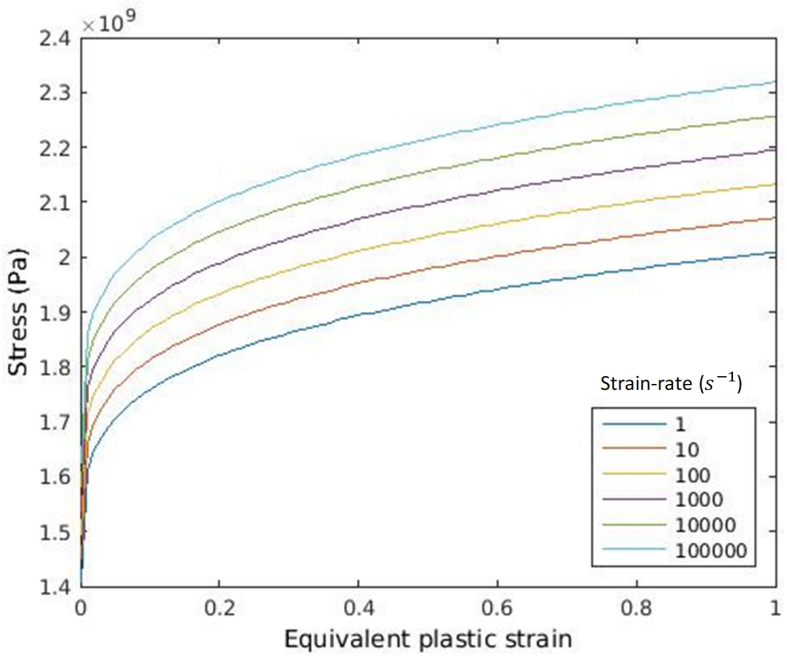

Figure 4.4: Stress vs. Equivalent plastic strain for varying strain-rates.

amount of mass proportional damping, also known as alpha damping, is applied on the DEM particles by default in Abaqus to reduce the noise generated by numerous opening and closing contact conditions.

4.3 Analysis

In this study, the simulation of the shot peening process on Almen strips is carried out in two steps. In the first step, Abaqus\Explicit is used to simulate a dynamic analysis of the shot peening process on the Almen strips with all the necessary boundary and contact conditions. Then the results of the dynamic analysis are transferred to Abaqus\Standard to simulate the springback analysis, to obtain the resulting arc-heights due to shot peening.

The explicit dynamic analysis uses a central difference scheme for a mechanical response [36], given by the equation.

$$\dot{u}^n_{i+\frac{1}{2}} = \dot{u}^n_{i-\frac{1}{2}} + \frac{\Delta t_{i+1} + \Delta t_i}{2} \ddot{u}^n_i \tag{4.5}$$

$$u^n_{i+1} = u^n_i + \Delta t_{i+1} \dot{u}^n_{i+\frac{1}{2}} \tag{4.6}$$

where u^n is the displacement or rotational degree of freedom of node n. And the subscript i denotes the increment number of the explicit step. $\dot{u}$ and $\ddot{u}$ represent the velocity and acceleration respectively. At the beginning of the increment the accelerations are calculated using equation 4.7

$$\ddot{u}^n_i = M^{-1} \cdot (F_i - L_i) \tag{4.7}$$

where M is the diagonal lumped mass matrix, F is the external load vector, and L is the internal force vector. These acceleration are then used in equation (4.5) and (4.6) to compute the velocities and displacements respectively. From the above equations it can be seen that the explicit analysis uses the values from the previous increments to advance the computations, thus requiring no iterations and it uses a diagonal mass matrix increasing the computational efficiency of the procedure [36].

The main drawback of the explicit analysis is that it integrates through time by using many small time increments. The central difference operator used in this analysis is conditionally stable which requires small time increments for accurate results. The stable time increments for the analysis is given by the equation (4.8)

$$\Delta t \leq \frac{2}{\omega_{max}} \tag{4.8}$$

where ω_{max} is the highest frequency of the system. In Abaqus, the stable time increments given in equation (4.8) is approximated as the smallest transit time for the dilatational wave to travel across the smallest element in the mesh.

$$\Delta t \approx \frac{L_{min}}{c_d} \tag{4.9}$$

where L_{min} is the length of the smallest element in the mesh and c_d is the dilatational wave speed given by

$$c_d = \sqrt{\frac{\lambda + 2\mu}{\rho}} \tag{4.10}$$

where ρ is the density of the material and λ, μ are the Lame's constants given in terms of Young's modulus E and Poisson's ratio ν, as shown in equation (4.11) and (4.12) respectively.

$$\lambda = \frac{E\nu}{(1+\nu)(1-2\nu)} \tag{4.11}$$

$$\mu = \frac{E}{2(1+\nu)} \tag{4.12}$$

Thus for a very fine mesh, the stable time increment is very small leading to large computational times. And also a dynamic analysis requires large amount of time to achieve steady state, whereas an equilibrium is achieved with a few increments in a static analysis. Hence, the obtained results from the Explicit analysis are then transferred to Abaqus\Standard to perform the springback analysis.

When the results are imported from an explicit dynamic analysis into a static analysis, the model will not initially be in static equilibrium. Initial out of balance forces must be applied on the deformed body in the dynamic analysis to achieve equilibrium in static [36]. And these out of balance forces are the result of any changes in the boundary and contact conditions from Abaqus\Explicit analysis to Abaqus\Standard analysis. The prompt removal of the initial out of balance forces will lead to convergence issues in static analysis. Hence, these forces are removed gradually until static equilibrium is achieved. During this process, the body will deform further, resulting in a redistribution of internal forces, thus forming a new stress state. The algorithm implemented automatically in Abaqus\Standard to remove the initial out of balance forces is given by the following steps [36],

1. The imported stresses from the explicit dynamic analysis are defined as the

initial stresses in the material at the start of the analysis.

2. An additional artificial stresses which are equal in magnitude to the imported stresses but opposite in sign are defined at each material point. The sum of the artificial stresses and the initial material point stress is zero, thus, creating zero internal forces at the beginning of the step.

3. These internal artificial stresses are removed linearly during the step time and by the end of the step the artificial stresses are completely removed. And the remaining stresses in the material will be the residual stress state associated with the static equilibrium.

Abaqus\Standard uses Newton's method as a numerical technique to solve nonlinear equilibrium equations. The basic formulation of the Newton's method is as follows,

$$F \cdot (u_i + c_{i+1}) = 0 \tag{4.13}$$

where F is the force component, u is the value of a variable in ith iteration and c denotes the difference between the solution in equation (4.13) and the exact solution of the discrete equilibrium equation given in equation (4.14)

$$F \cdot u = 0 \tag{4.14}$$

Using Taylor series expansion of equation (4.13) and neglecting all but the first two terms, we have

$$K_i \cdot c_{i+1} = -F_i \tag{4.15}$$

where K is the Jacobian matrix give by

$$K_i = \frac{\partial F}{\partial u} \cdot u_i \tag{4.16}$$

and the iteration continues using the next approximation to the solution given by equation (4.17)

$$u_{i+1} = u_i + c_{i+1} \tag{4.17}$$

Abaqus checks for the convergence of the Newton's method by ensuring that the values of the force components (F) and c are sufficiently small.

4.4 Contact Algorithm

Shot peening involves a large number of particles interacting with each other as well as with the target. To simulate these interactions in Abaqus, a contact model is to be defined which prevents the complete penetration of one body into another and also provides frictional resistance between the sliding bodies. In general, Abaqus\Explicit offers two approaches for defining contacts. They are the contact pair approach which enforces the contact more strictly (no penetration) and has more restrictions on the surfaces that can be used. And the general contact approach, which has very few restrictions on the types of surfaces compared to the contact pair approach and also it is the only option for enforcing contacts involving DEM particles. Hence, the general contact algorithm is used in this study.

In the general contact approach, Abaqus requires the user to define a master and a slave surface. The surface with a higher stiffness of the two interacting bodies is to be defined as a master surface. And the surface with lower stiffness is defined as slave surface. The master-slave assignment allows one surface (master) to penetrate into another surface (slave). In this work, the shots are chosen as the master surface as they are modeled as rigid bodies and the strip is defined as the slave surface. An illustrative figure showing the master and slave surfaces is shown in figure 4.5.

Further, Abaqus\Explicit uses two different methods to enforce constraints [36]. They are the kinematic contact algorithm which uses a kinematic predictor/corrector contact algorithm to enforce the contact constraints (no penetrations allowed) strictly.

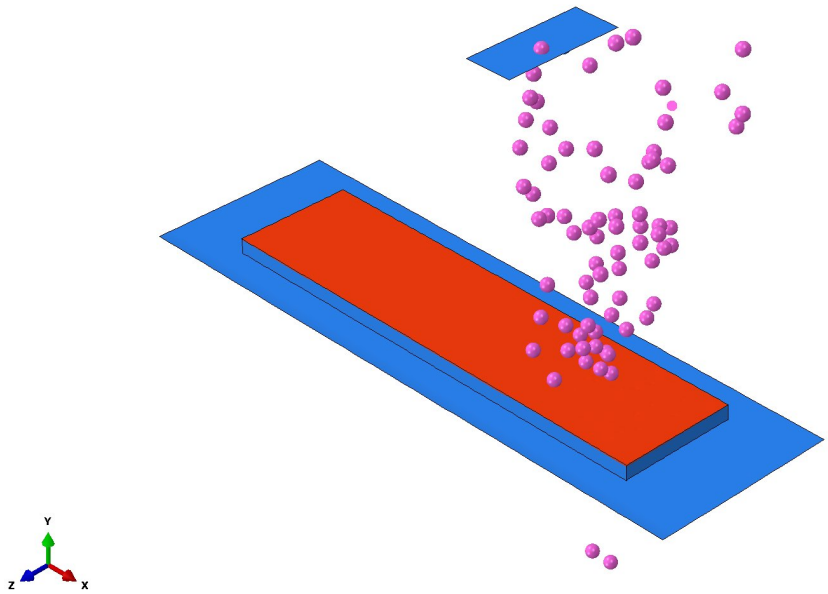

Figure 4.5: Contact between the DEM particles and the Almen strip.

And the penalty contact algorithm which has weaker enforcement of contact constraints but allows the treatment of a more general type of contact which involves multiple contacts per node and contact between rigid bodies. The general contact approach used in this study always uses the penalty contact algorithm by default. In this approach, the algorithm searches for the slave node penetrations in the current configuration and calculates the contact forces as a function of the penetration distance. And these calculated forces are then applied to the slave nodes to oppose the penetration, while an equal and opposite forces act on the master surface resulting in equivalent forces and moments on the rigid body. One of the drawbacks of the penalty algorithm is that it introduces additional stiffness into the model which will influence the stable time increments. Abaqus automatically chooses the spring stiffness that relates the contact force to the penetration distance, such that the effect on time increment is minimal.

To model the contact between the DEM particles, Abaqus requires the particles to be explicitly included in the general contact as element based surfaces using contact

inclusions. Hence a surface is defined to include all the particles, and a contact condition is defined between the particles surface and the top surface of the Almen strip. Also, a similar contact condition is defined between the bottom surface of the strip and the top surface of the rigid support. Further, in Abaqus, users are required to define a normal and tangential contact property between the interacting surfaces. Hence, in this study, a hard contact relationship is defined in the normal direction, and the frictional properties are defined in the tangential direction. The hard contact approach defines the contact pressure as a function of the overclosure of the surfaces, and it minimizes the penetration of the slave surface into the master surface at the constraint locations. In this method, the surfaces separate when the contact pressure reduces to zero. The frictional properties in the tangential direction are provided to eliminate any frictional slip when the surfaces are in contact. A classical version of the isotropic Coulomb's friction model is used in Abaqus. This model relates the maximum allowable frictional stress across an interface to the contact pressure between the contacting bodies [36], as shown in equation (4.18)

$$\tau_{crit} = \mu p \tag{4.18}$$

τ_{crit} is the critical shear stress at which the surfaces start sliding, p is the contact pressure and μ is the coefficient of friction. Abaqus assumes that no relative motion occurs between the interacting bodies if the equivalent shear stress (τ_{eq}), given in equation (4.19), is less than the critical stress (τ_{crit}).

$$\tau_{eq} = \sqrt{\tau_1^2 + \tau_2^2} \tag{4.19}$$

τ_1 and τ_2 are the shear stress components of the interacting bodies.

As seen in the literature, there have been few studies that analyzed the influence of tangential friction on the compressive residual stresses in shot peening. Han et al. [37]

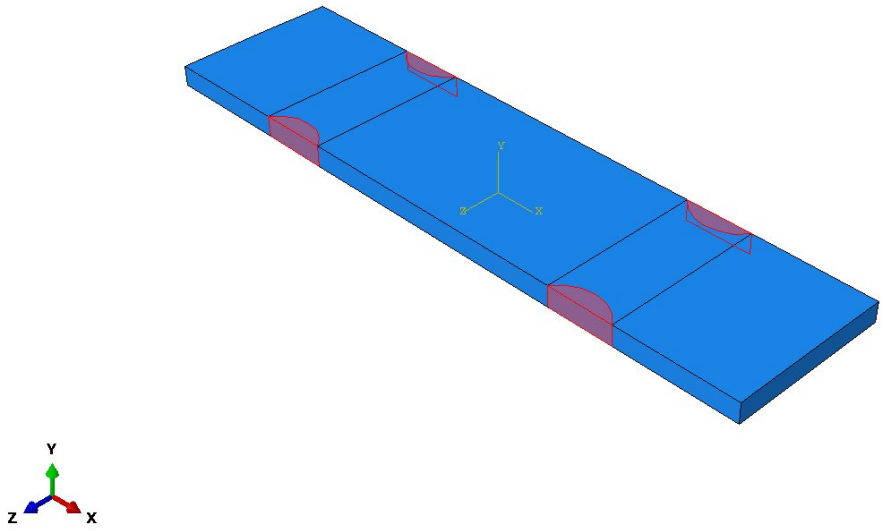

Figure 4.6: The highlighted areas are fully constrained to represent the action of the bolts on the strip.

and Meguid et al. [25] analyzed the effect of coefficient of friction on the development of compressive residual stresses. They showed that the resulting compressive residual stresses are increased with an increase in the coefficient of friction and converge to steady value for a friction coefficient greater than or equal to 0.2. Hence, a Coulomb friction coefficient of $\mu = 0.25$ is used in this study, for the contact between the shots and the strip.

4.5 Boundary and Initial Conditions

As described in the first chapter, the Almen intensity tests are carried out by constraining the Almen strips on a holder with the help of four bolts. To simulate the similar conditions, the strip is placed on a rigid support, which is fully constrained and the bolt conditions are simulated by fully constraining the appropriate regions on the strip that are in contact with the bolts, as shown in figure 4.6.

For the distribution of shots over the Almen strip, the particle generator is translated over the strip by defining a displacement boundary condition, as shown in figure

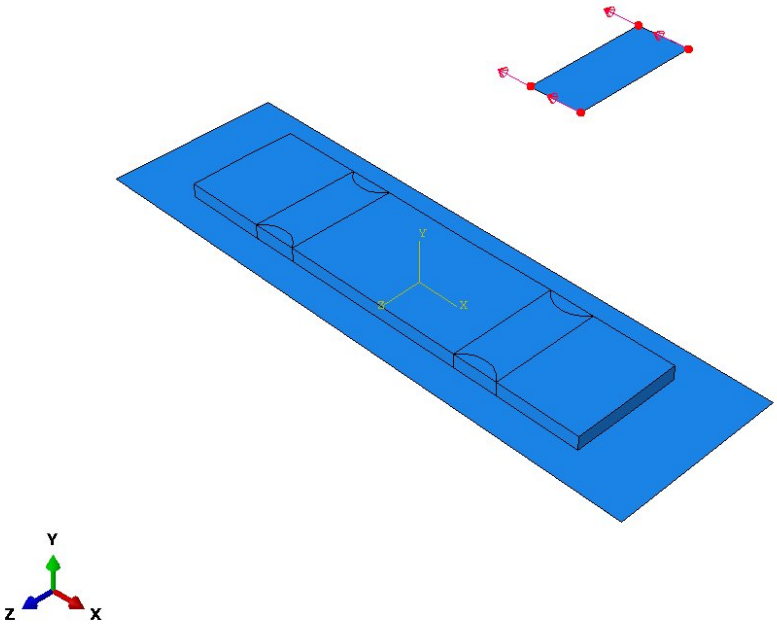

Figure 4.7: The particle generator is constrained to move in only the x direction.

4.7. Initially, the particle generator is placed at the right end of the strip and provided a displacement in the negative x-direction. As the particle generator reaches the other end (which is counted as a single pass), the course of the particle generator movement is reversed, and the process is continued until the required number of transitions are obtained. In Abaqus, these displacements are provided as a function of step time, by defining an amplitude data as shown in table 4.4.

Table 4.4: Amplitude function for displacements of particle generator.

Time (s)	Amplitude
0.005	-0.069
0.01	0.0
0.015	-0.069
0.02	0.0
0.0201	0.01

Table 4.5: Amplitude function for initial velocity.

Time (s)	Amplitude
0.0	80
0.0001	80

Table 4.6: Amplitude function for mass flow rate.

Time (s)	Amplitude
0.0	4.566E+03
0.02	4.566E+03
0.0201	0.0

The velocity and mass flow rate of the DEM particles are defined at the particle generator. In this study, the velocity is considered to be constant and is defined as a function of step time as given in table 4.5. In Abaqus, the mass flow rate ($\dot{M}_s$) is defined using equation 4.20,

$$\dot{M}_s = \frac{M}{t \cdot A} \tag{4.20}$$

where t is the time in which the specified amount of shot should be generated, A is the area of the inlet and M is the total mass of the shots, given by

$$M = m \cdot N \tag{4.21}$$

m is the mass of individual shot particle and N is the number of shots. For example, in this study, for a shot with diameter of 2 mm, 200 shots are considered to be generated from the inlet in 0.01 sec i.e. in single pass. Hence, using equation (4.20) and (4.21) the required mass flow rate is calculated to be 4566 Kg/(sec.m^2). In Abaqus, the

mass flow rate is defined as function of step time by using an amplitude function as shown in table 4.6.

4.6 Element Type and Meshing

The selection of element type and the structure of the mesh are the most critical aspects of finite element analysis. Abaqus provides a wide variety of elements to chose from, whose behavior is characterized based on their family (continuum, rigid, shell, truss etc.), degrees of freedom (translations, rotations, temperatures etc.), number of nodes (depend on the geometry and the type of interpolation, i.e. linear or quadratic), formulation (mathematical theory describing the elements behaviour) and integration. And each of these elements is given a unique name depending on the aspects as mentioned above [36].

The simulation of the shot peening process requires a stress analysis which uses the stress or displacement elements in Abaqus, which are limited to translational and rotational degrees of freedom. These elements are used for modeling the complex nonlinear behavior involving contact, plasticity, and large deformations. Stress elements are further classified into different element families such as continuum elements, structural elements, rigid elements, etc. In this study, three-dimensional solid continuum elements are used to model the Almen strip. Based on the geometry the solid continuum elements are again classified into tetrahedral (triangular) or hexahedral (brick) elements. The tetrahedral elements are geometrically flexible and can be used to model complex shapes, but for accuracy, second-order elements should be used. Whereas in case of hexahedral elements a good mesh or well-structured mesh will provide a solution of equivalent accuracy at less cost and they also have a better convergence rate than the tetrahedral elements.

Abaqus uses two types of Gauss integration schemes in the formulation of the stiffness matrix [36]. They are the full integration scheme where all the integration points are used in the evaluation of the stiffness matrix and the reduced integration

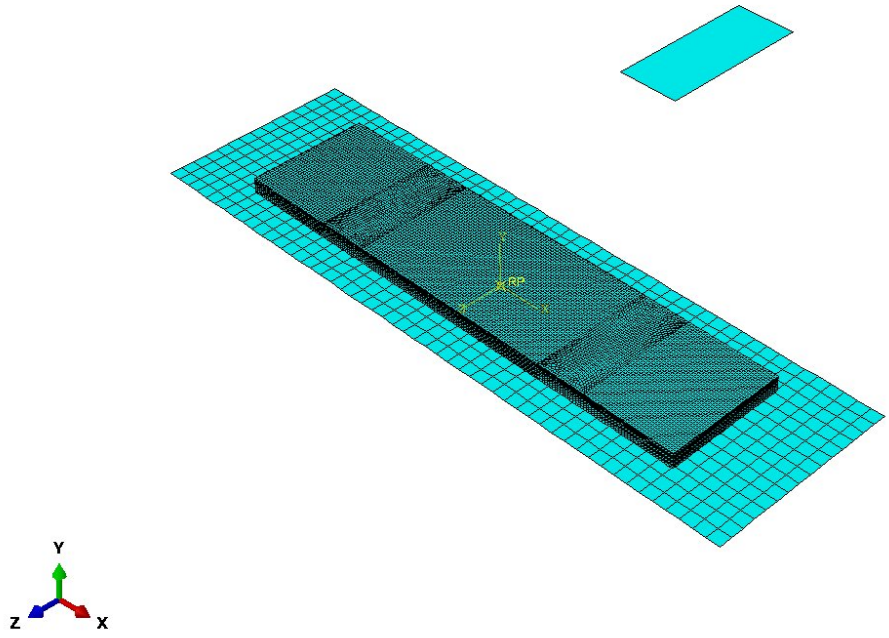

Figure 4.8: Mesh.

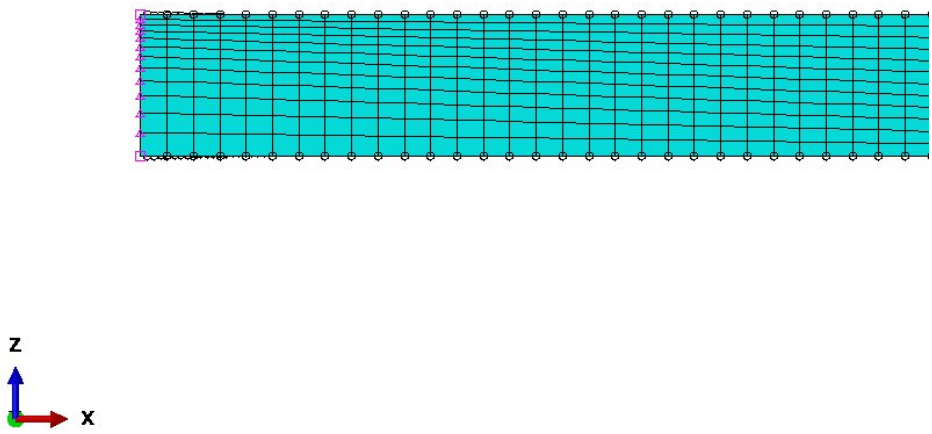

Figure 4.9: Biased mesh.

scheme where relatively less number of Gaussian points or integration points are used in the formation of the element stiffness matrix. The use of more number of integration points in the full integration technique leads to more accurate results but also increases the computational cost of the analysis. For example, a fully integrated, second-order, 20-node three-dimensional element requires integration at 27 points, while the reduced-integration version of the same element only uses 8 points and, therefore, costs less than 30% of the fully integrated version [36]. On the other hand, finite element formulations of displacement analysis always over-estimates the stiffness matrix, and the use of slightly less accurate reduced integration technique will approximate the analysis to real-life behavior. But the use of reduced integration technique on linear elements may lead to instability due to the stiffness matrix being zero, i.e., the use of reduced integration may lead to few elements with zero stiffness or resistance to the deformations and will lead to the excessive distortions of the mesh, thus destabilizing the analysis [36]. This effect is also known as hourglassing. Abaqus provides few different formulations that can be used to control the hourglass effect.

In this study, considering the computational cost, approximately around 90,000 eight node hexahedral elements (C3D8R) with reduced integration are used to model the Almen strip, as shown in figure 4.8. An enhanced hourglass control is used to control the hourglassing effect. A biased mesh along the depth of the strip, as shown in figure 4.9, with finer elements at the interacting or top surface of the strip, is used. And to model the shots, Abaqus uses discrete particle elements (PD3D) which are associated with a discrete section providing the density and particle radii.

CHAPTER 5: RESULTS AND VERIFICATION

5.1 Results

The results from the explicit analysis are transferred to the Abaqus\Standard to perform the springback analysis which is carried out in two steps. In the first step, static analysis is performed on the constrained strip to damp out any vibrations and also to simulate the state of completing the peening operation just before removing the strip from the Almen holder. And then in the second step, the constraints or bolt conditions on the strip are removed. Additionally, appropriate boundary conditions are added to the strip to prevent any rigid body motions. At the end of the second step, the strip bends in the direction of peening, forming an arc similar to that observed in the experiments. The isometric and side views of the deflected Almen strip are shown in figure 5.1 and figure 5.2 respectively.

The normal stress distribution in the x-direction (S_{11}), on the top or peened surface of both the constrained and unconstrained strip is shown in figure 5.3 and figure 5.4 respectively. In the constrained state, the top surface of the strip is prominently induced with compressive residual stresses, with some tensile stresses at the edges of the strip. And when the constraints are removed, the stresses become comparatively more tensile on the surface. Similarly, figure 5.5 and figure 5.6 show the normal stress distribution (S_{11}) on the bottom surface of the strip in both constrained and unconstrained states respectively. In this case, in the constrained state, the stresses are more tensile near the bolts and compressive at the center of the strip, but in the unconstrained state, the stresses are predominantly compressive in the bottom surface of the strip. This variation of the stresses in the strip is due to the constraints on the strip which induce unbalanced stress during the shot peening process [38], and

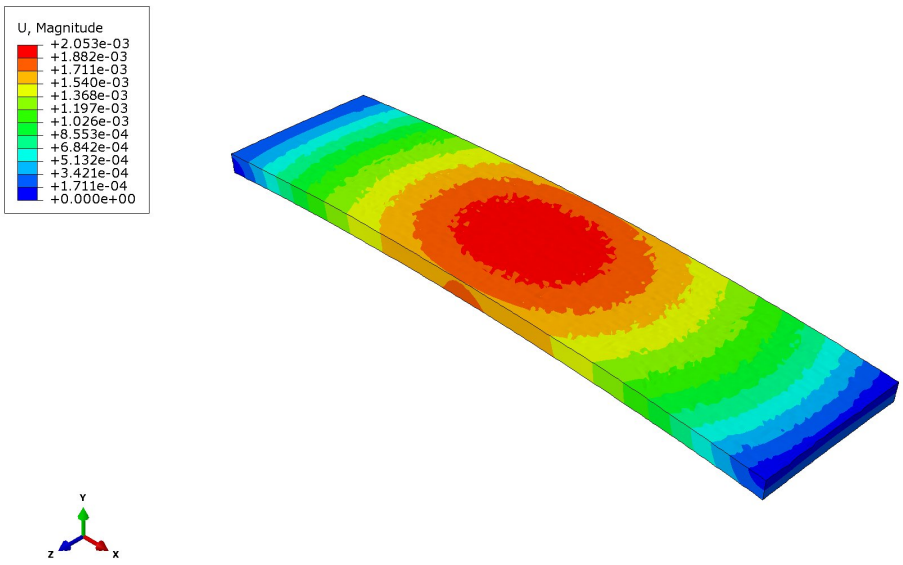

Figure 5.1: Deflection of Almen strip (isometric view).

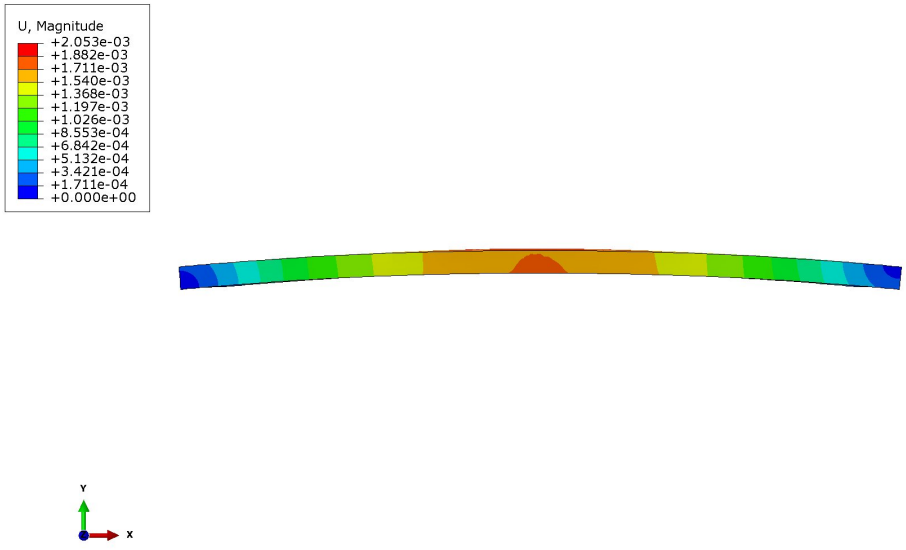

Figure 5.2: Deflection of Almen strip (side view).

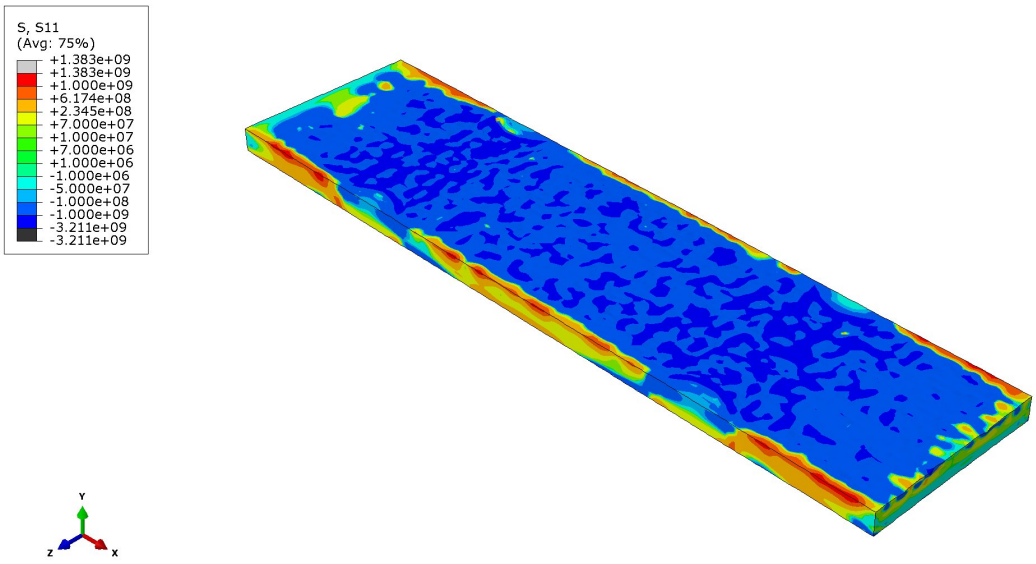

Figure 5.3: Normal stress distribution (S_{11}) in the top surface (constrained state).

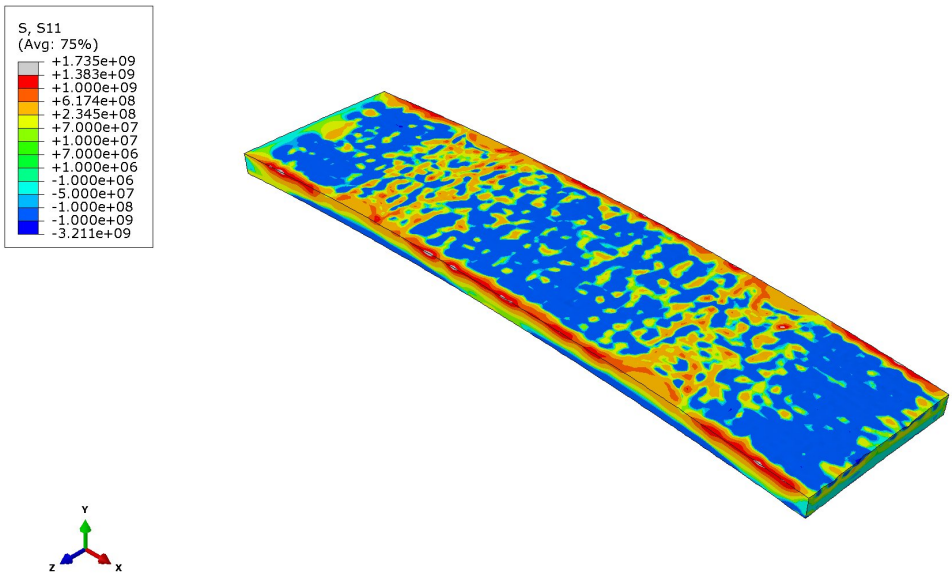

Figure 5.4: Normal stress distribution (S_{11}) in the top surface (unconstrained strip).

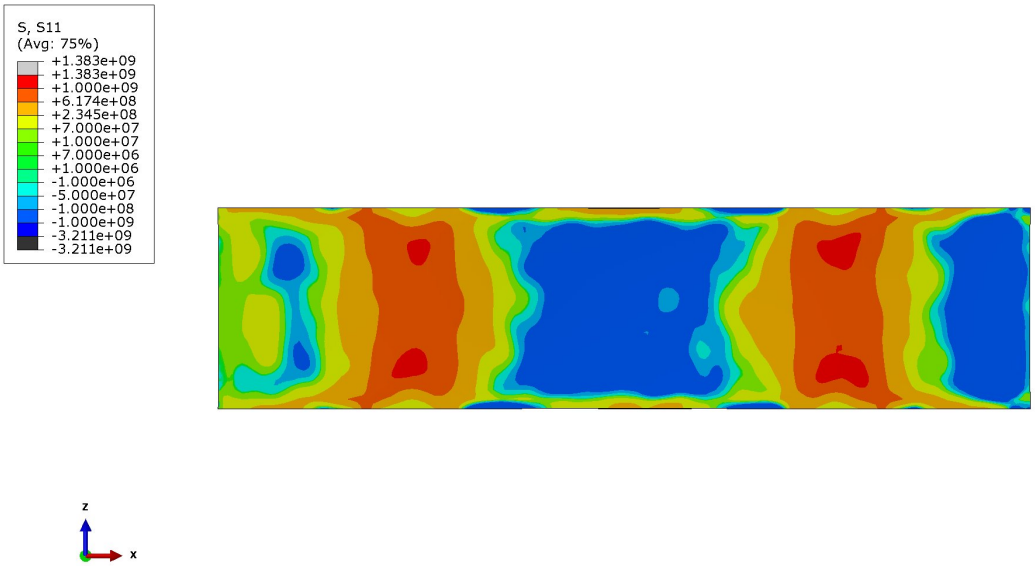

Figure 5.5: Normal stress distribution (S_{11}) in the bottom surface (constrained state).

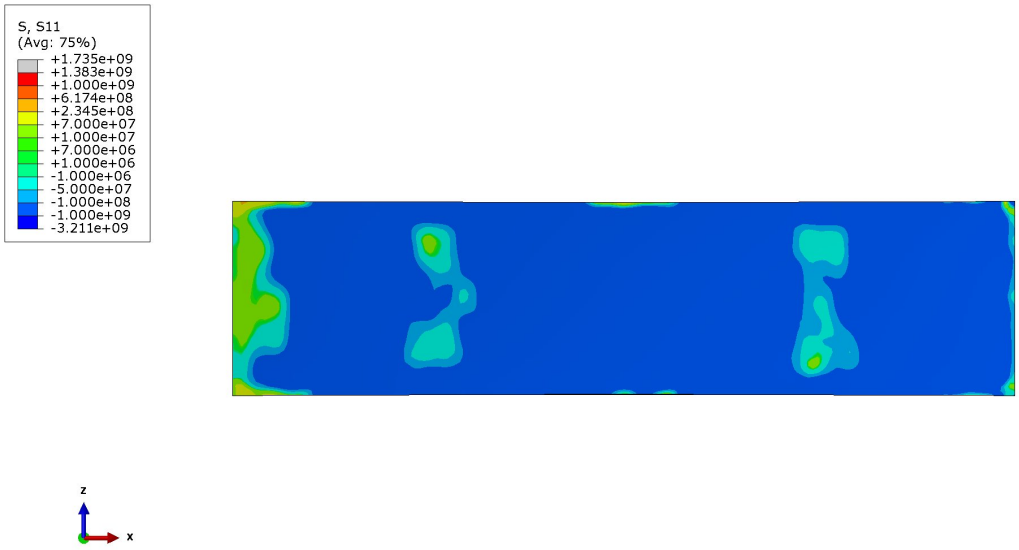

Figure 5.6: Normal stress distribution (S_{11}) in the bottom surface (unconstrained strip).

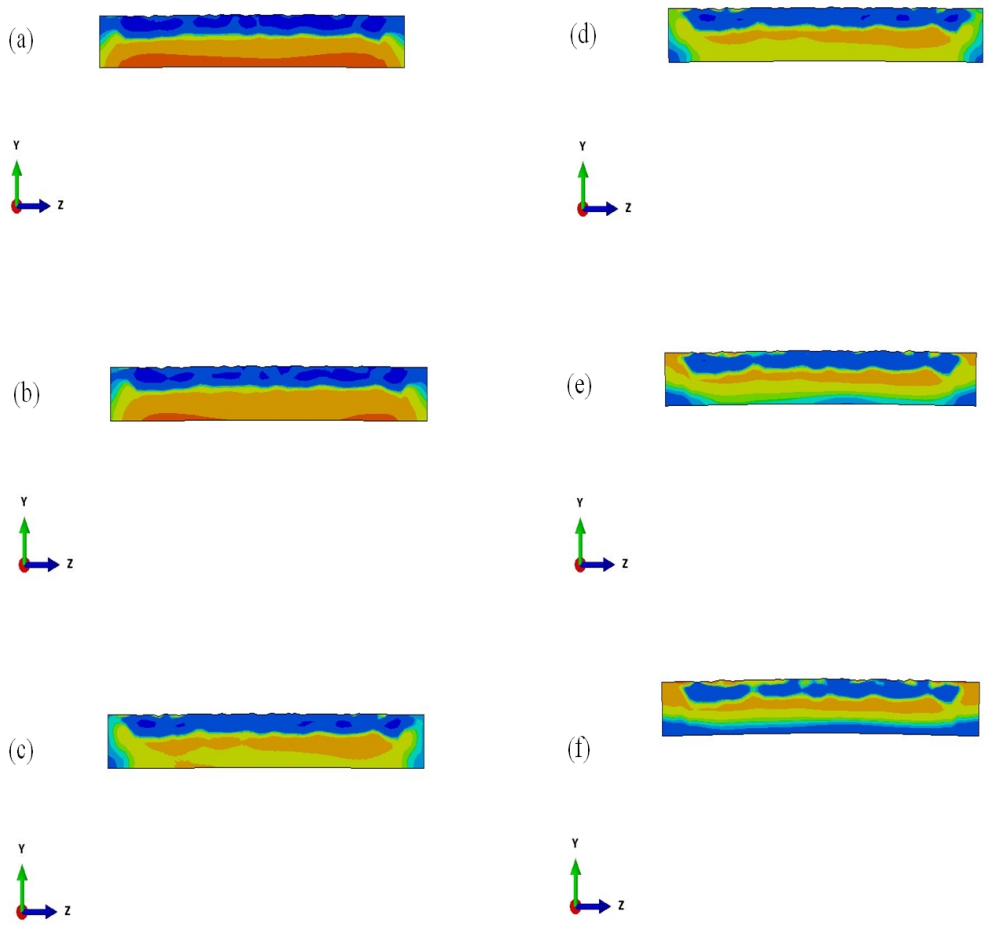

Figure 5.7: Stress (S_{11}) redistribution during the springback analysis.

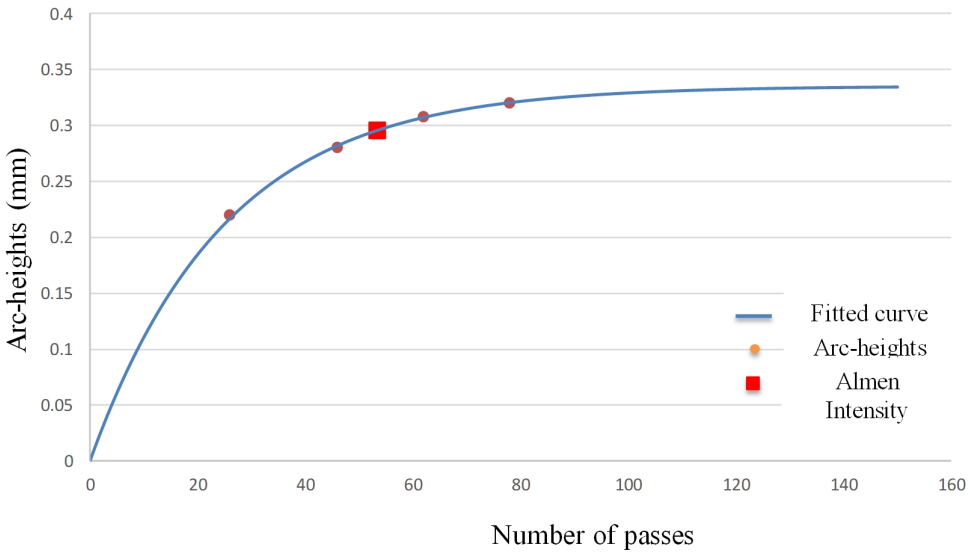

Figure 5.8: Saturation curve.

once these external constraints are removed, the stresses are redistributed until an equilibrium is reached. Figure 5.7 shows the normal stress distribution along the depth in a cross-section of the strip (near the bolts) during the springback analysis. It is observed that at the beginning of the springback analysis (figure 5.7(a)), the stresses are compressive on the peened surface and tensile on the bottom surface. And when the constraints are removed, the stresses start to redistribute and reach an equilibrium state at the end of the springback analysis (figure 5.7(f)), where the compressive stresses in the top surface are replaced with tensile residual stresses with subsurface compressive stresses and the tensile stresses on the bottom surface are completely replaced with compressive residual stresses.

In the Almen strip tests, the arc heights are measured at a distance of 15.87 mm from the blots. So, in case of the simulations, the height at the center of the strip relative to the height at the bolts is considered as the arc-height. To obtain the Almen intensity, the simulations are carried out for a different number of peening passes, and the resulting arc-heights are plotted against their respective number of peening passes, as shown in figure 1.4. A two-parameter curve fitting program developed by David

Kirk, given by the equation (5.1), is used to obtain the Almen intensity [39].

$$h = a(1 - e^{-bt}) \tag{5.1}$$

where h is the arc-height (mm), t is the peening time (number of passes in this study) and a,b are the fitting parameters.

The effect of the number of peening passes on the stress distribution along the thickness of the strip at its center in both the constrained and the unconstrained state is shown in figure 5.9 and figure 5.10 respectively. In the constrained state, as the number of peening passes increased the depth of the compressive layer and the magnitude of the compressive stresses increased. But in the unconstrained state, the magnitude of the compressive stresses on the surface decreased while the magnitude of the tensile stresses increased in the subsurface layers with an increase in the number of peening passes. And also the stresses became more compressive at the bottom of the strip. In both cases it is observed that the magnitude and the depth of the compressive layers saturate after a certain number of peening passes.

In Figures 5.11 and 5.12, the effect of number of peening passes on the equivalent plastic strains along the thickness of the strip in both constrained and unconstrained states is shown respectively. It is observed that the permanent plastic strain exists in the top layers of the strip with a maximum magnitude in the subsurface and gradually reducing to zero along the depth. Further, comparing figures 5.11 and 5.12, it is found that the springback analysis doesn't have any effect on the plastic strains.

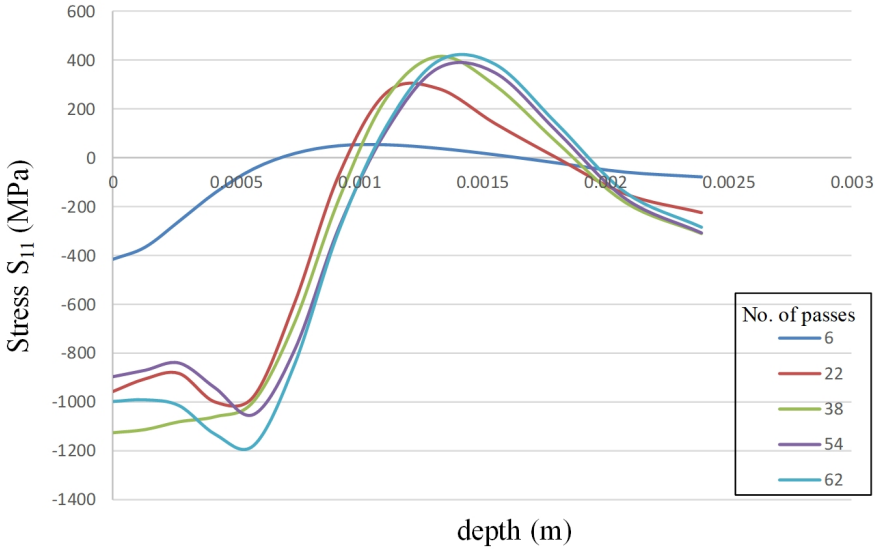

Figure 5.9: Effect of number of peening passes on the stresses in the constrained strip.

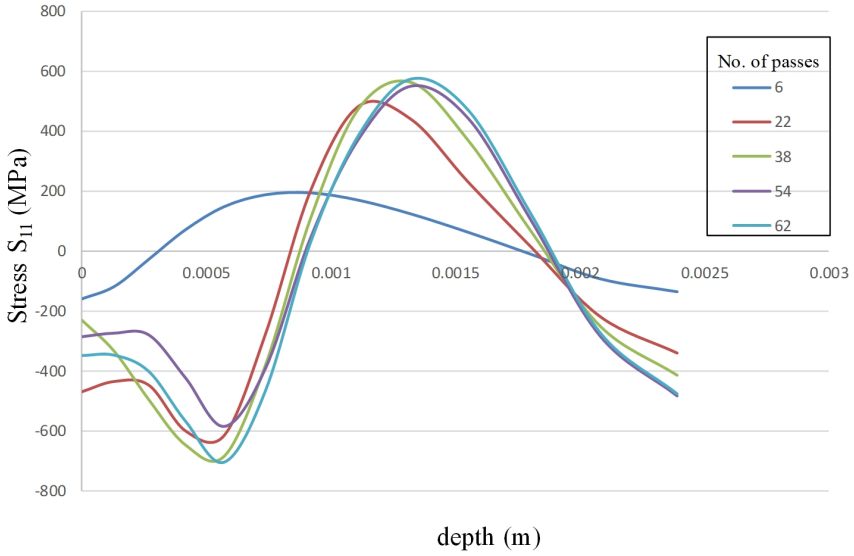

Figure 5.10: Effect of number of peening passes on the stresses in the unconstrained strip.

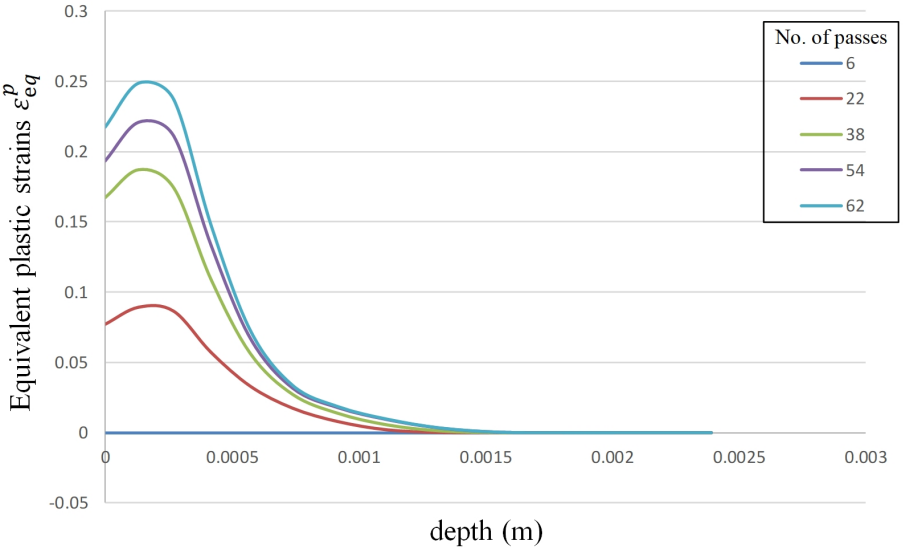

Figure 5.11: Effect of number of peening passes on equivalent plastic strains (constrained).

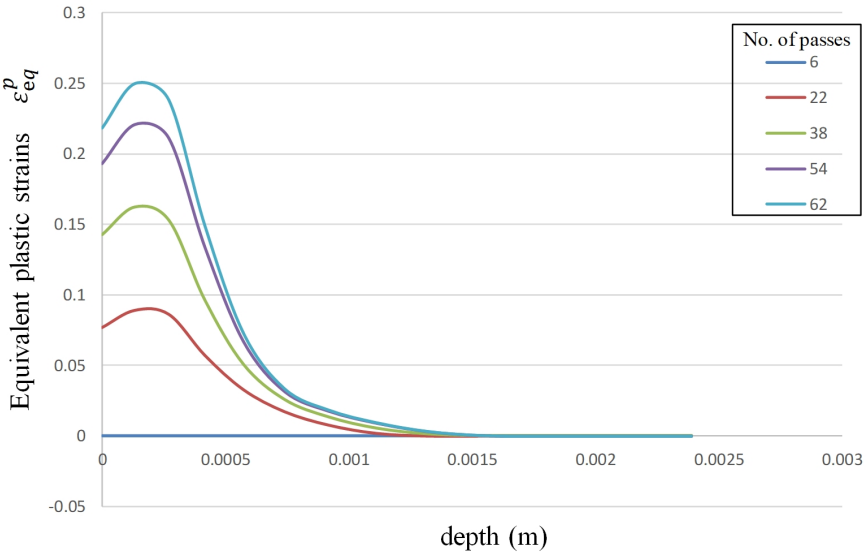

Figure 5.12: Effect of number of peening passes on equivalent plastic strains (unconstrained).

5.2 Verification

The analytical model developed by Miao et al. [14] has been used in this study to verify the numerical model. They used the Hertz theory of elastic contact along with a simplified elasto-plastic material model to predict the Almen intensity. The sequence of steps involved in deriving the analytical model are as follows.

First, the maximum value of the pressure (p_0) during the elastic impact between the shot and the target is calculated from the Hertz theory of elastic contact as

$$p_0 = \frac{1}{\pi}\left[40\pi k\rho E_H^4 V^2\right]^{\frac{1}{5}} \tag{5.2}$$

where, ρ is the density of the shot, V is the shot velocity, and k is the elastic dissipation coefficient. The elastic dissipation coefficient k is assumed to be constant with a value of 0.8. Then, the maximum contact radius (a_e) is calculated as

$$a_e = \frac{D}{2}\left[\frac{5}{4}\pi k\rho\frac{V^2}{E_H}\right]^{\frac{1}{5}} \tag{5.3}$$

where D is the shot diameter and E_H is the equivalent Young's modulus given by

$$\frac{1}{E_H} = \frac{1-\nu_s^2}{E_s} + \frac{1-\nu_T^2}{E_T}. \tag{5.4}$$

In this expression, E_s and ν_s are respectively the Young's modulus and Poisson's ratio of the shot material, and E_T and ν_T are respectively the Young's modulus and Poisson's ratio of the target material. Using equations (5.2) and (5.3), the principal stresses at the center of the contact area of the target are calculated as follows:

$$\sigma_x^e = \sigma_y^e = -p_0\left[-\frac{1}{2}A(z) + (1+\nu_T)B(z)\right] \tag{5.5}$$

and

$$\sigma_z^e = -p_0 A(z) \tag{5.6}$$

with $A(z)$ and $B(z)$ being defined by

$$A(z) = \left[1 + (\frac{z}{a_e})^2\right]^{-1} \tag{5.7}$$

and

$$B(z) = 1 - \frac{z}{a_e} tan^{-1}\left(\frac{a_e}{z}\right). \tag{5.8}$$

Here, z is the thickness under consideration of the target body. Using the principal stresses from equation (5.5) and (5.6), the von Mises equivalent stress (σ_i^e) is calculated as follows,

$$\sigma_i^e = \frac{1}{\sqrt{2}}\left[(\sigma_x^e - \sigma_y^e)^2 + (\sigma_y^e - \sigma_z^e)^2 + (\sigma_z^e - \sigma_x^e)^2\right] \tag{5.9}$$

and the equivalent strain (ϵ_i^e) is given by equation 5.10

$$\epsilon_i^e = \frac{\sigma_i^e}{E_T} \tag{5.10}$$

Then for the elasto-plastic analysis of the loading process, the plastic strains are calculated using the strain field given by equation (5.9),

$$\epsilon_i^p = \begin{cases} \epsilon_i^e & for\ \epsilon_i^e \leq \epsilon_s \\ \epsilon_s + \alpha(\epsilon_i^e - \epsilon_s) & for\ \epsilon_i^e > \epsilon_s \end{cases} \tag{5.11}$$

where α is defined as the ratio of the radius of maximum plastic indentation (a_p) to the radius of the maximum elastic contact (a_e) and ϵ_s is the strain corresponding to the yield stress (σ_s) of the target material. And the radius of maximum plastic indentation is given by equation (5.12).

$$a_p = \frac{D}{2}\left[\frac{8\rho V^2}{9\sigma_s}\right]^{\frac{1}{4}} \tag{5.12}$$

The strains calculated in equation (5.11) are then used to calculate the stresses, as shown in equation (5.13),

$$\sigma_i^p = \begin{cases} \sigma_i^e, & \epsilon_i^p < \epsilon_s, \\ \sigma_s + H(\epsilon_i^p - \epsilon_s), & \epsilon_s \leq \epsilon_i^p < \epsilon_b, \\ \sigma_b, & \epsilon_i^p >= \epsilon_b. \end{cases} \tag{5.13}$$

Here, H is the linear strain hardening parameter, σ_b is the ultimate tensile stress of the target material and ϵ_b is the strain corresponding to the ultimate stress. Next, the transresidual stresses, i.e., the stresses in the target material due to successive loading and unloading of a single shot, are calculated by assuming that the target material is an isotropic hardening material.

$$\sigma_x^t = \sigma_y^t = \begin{cases} 0, & \sigma_i^e < \sigma_s, \\ \frac{1}{3}(\sigma_i^p - \sigma_i^e), & \sigma_s \leq \sigma_i^e \leq 2\sigma_i^p, \\ \frac{1}{3}\left(-\sigma_i^p - H\alpha\frac{(\sigma_i^e - 2\sigma_i^p)}{E_T}\right), & \sigma_i^e > 2\sigma_i^p \end{cases} \tag{5.14}$$

and

$$\sigma_z^t = -2\sigma_x^t. \tag{5.15}$$

By using the above equations, the induced stresses (σ_{ind}) corresponding to the 100% peening coverage are evaluated as follows,

$$\sigma_{ind} = \frac{1+\nu}{1-\nu}\sigma_x^t \tag{5.16}$$

These induced stresses are then used to calculate the bending moments (M_x) applied

by the bolts on the Almen strip, given in equation (5.17).

$$\int_0^h \sigma_{ind} \left(\frac{h}{2} - z \right) b dz + M_x = 0 \tag{5.17}$$

where b is the width and h is the thickness of the strip. The resulting arc heights are then calculated using equation (5.18)

$$\text{Arc Height} = \frac{3 M_x l_m^2}{2 E b h^3} \tag{5.18}$$

where l_m is the reference distance for measuring the Almen intensity.

The Almen intensities obtained from the numerical model as well as the analytical model for different impact velocities are shown in table 5.1. The maximum difference observed in the intensities is around 17% in case of low velocity and around 6% for higher velocities. The possible explanations for this difference are, the friction effect between the shots and the target is neglected in the analytical model whereas friction is considered in case of the simulations. And also the elastic dissipation coefficient, which depends on various peening parameters, is assumed to be constant in case of the analytical model.

Table 5.1: Comparison of simulated Almen intensities with analytical model.

Velocity (m/s^2)	Arc Heights (mm)	
	Simulations	Analytical
80	0.30	0.32
70	0.28	0.30
60	0.22	0.28

CHAPTER 6: PARAMETRIC STUDY

The numerical model described in the previous chapters is used to study the effect of various process parameters such as shot velocity, the angle of impact and shot size on the field variables, i.e., normal stress component in the x-direction and equivalent plastic strains, and Almen intensities. In this study, during the analysis of the influence of a parameter on the field variable, all the other parameters are considered to be constant. And in this study, the mass flow rate is assumed to be constant in all cases and is considered to be 4566 kg/s.m^2. The stresses and plastic strains for different cases are compared by measuring their values at the center of the strip along its thickness.

6.1 Shot Velocity

The effect of different shot velocities is analyzed by considering the angle of impact to be perpendicular, and the shot size to be 2 mm in diameter. Three different shot velocities 60, 70 and 80 m/sec are considered in this study. Figure 6.1 shows the Almen intensities obtained for different shot peening velocities. It is observed that the Almen intensity increases with the increase in the shot velocity.

Figures 6.2 and 6.3 shows the stress profile along the thickness of the strip for different velocities in both constrained and unconstrained states respectively. In case of the constrained strip, the top layers of the strip are induced with compressive stresses with maximum compressive stress occurring below the top surface. It is also observed that as the shot velocity increased the depth of the induced compressive stress also increased. In case of the unconstrained strip, the magnitude of the compressive stresses decreased in the top surface and in case of low velocity the compressive stresses in the

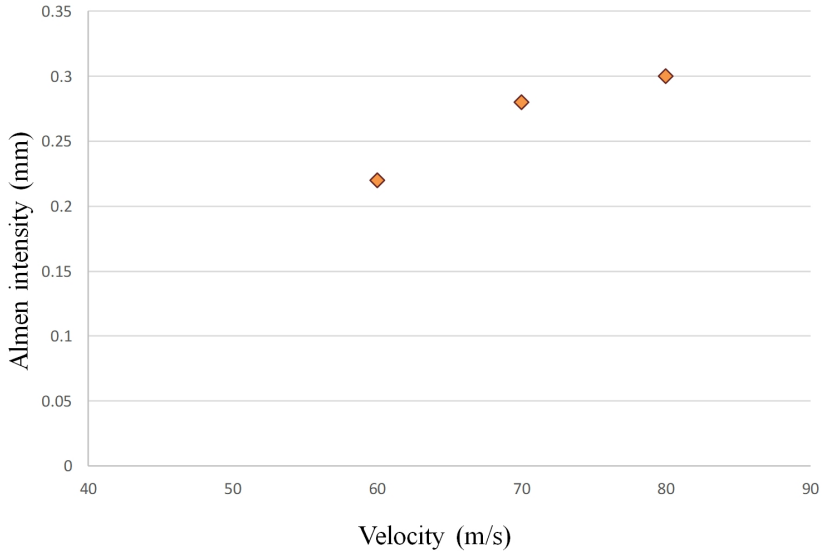

Figure 6.1: Effect of impact velocity on the Almen intensity.

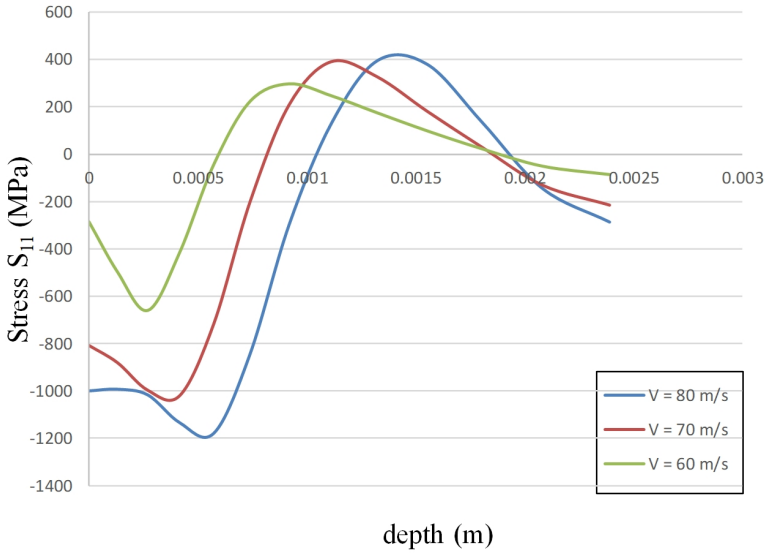

Figure 6.2: Effect of impact velocity on the induced stresses in constrained strip.

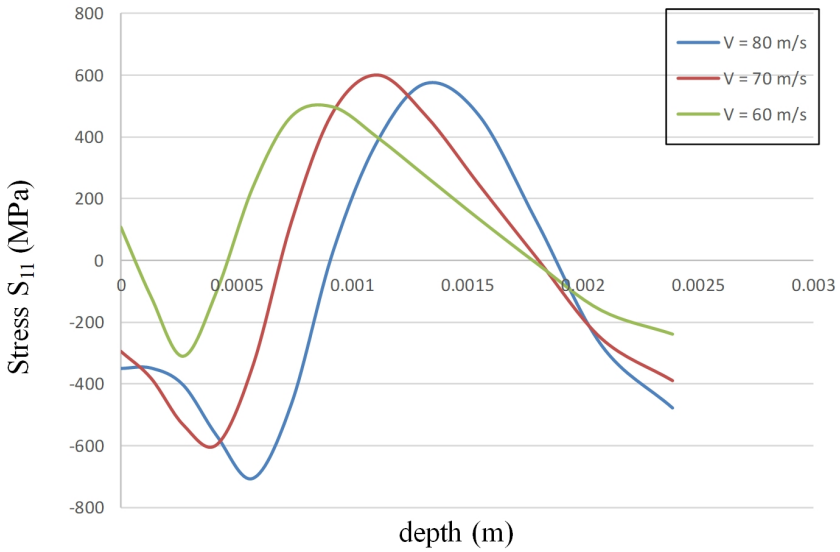

Figure 6.3: Effect of impact velocity on the residual stresses in unconstrained strip.

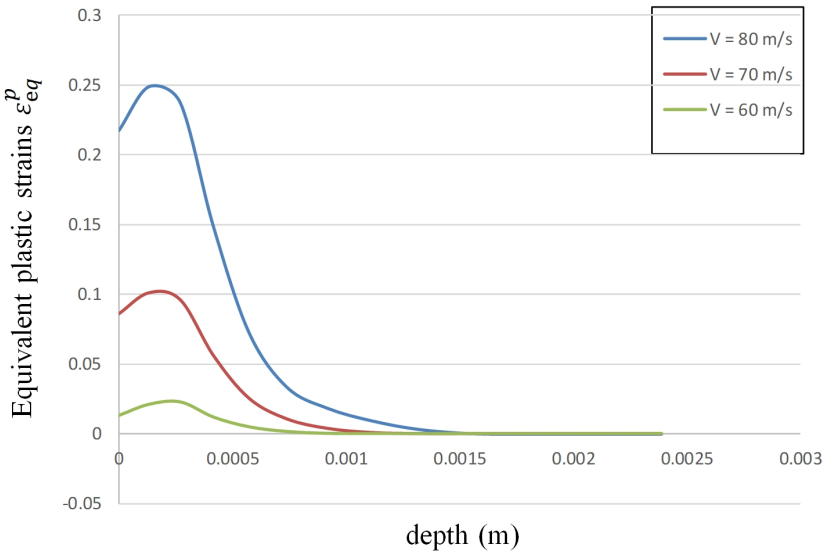

Figure 6.4: Effect of impact velocity on the equivalent plastic strains.

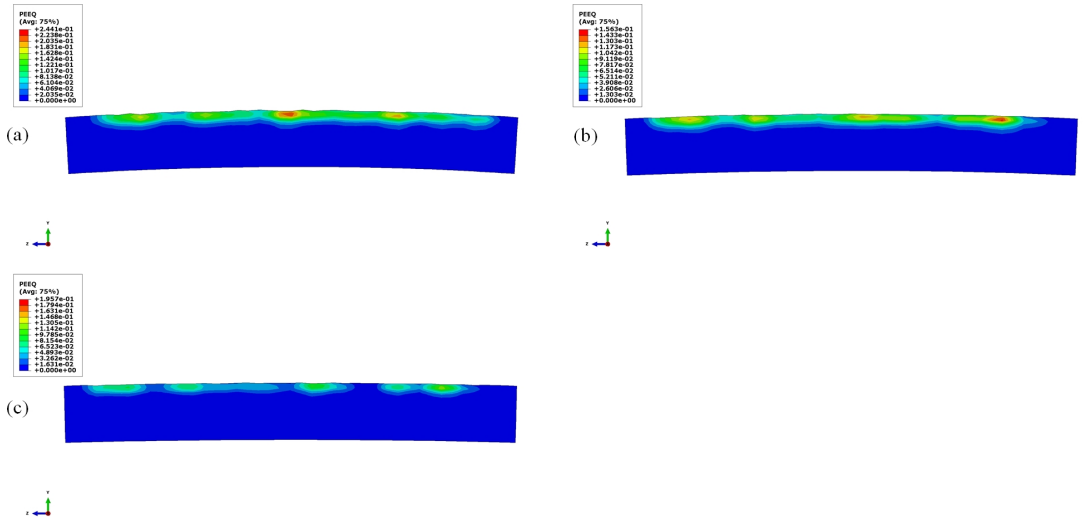

Figure 6.5: Equivalent plastic strains in a cross section vs velocity (a) 80 m/s, (b) 70 m/s & (c) 60 m/s.

top surface are replaced with tensile residual stresses. As the shot velocity increased the magnitude of the compressive residual stresses in the bottom surface of the strip also increased.

As shown in figure 6.4, the magnitude and the depth of the equivalent plastic strains increased with the increase in shot velocity. Figure 6.5 shows the distribution of equivalent plastic strains in the cross-section of the Almen strip at its center for various shot velocities. And the figure 6.6 shows that the maximum equivalent plastic strain in the Almen strip increased with the increase in the shot velocity.

6.2 Angle of Impact

In this study, the effect of three different impact angles ($90°, 75°$ *and* $60°$) on the Almen strip is analyzed. And in this case, the shot velocity is considered to be 80 m/s and the shot diameter to be 2 mm. The Almen intensities obtained for different impact angles are as shown in figure 6.7. It is observed that the Almen intensities decreased with the decrease in the angle of impact.

Figure 6.8 shows the variation of the induced normal stresses in a constrained strip through its thickness for different impact angles. It is observed that as the angle

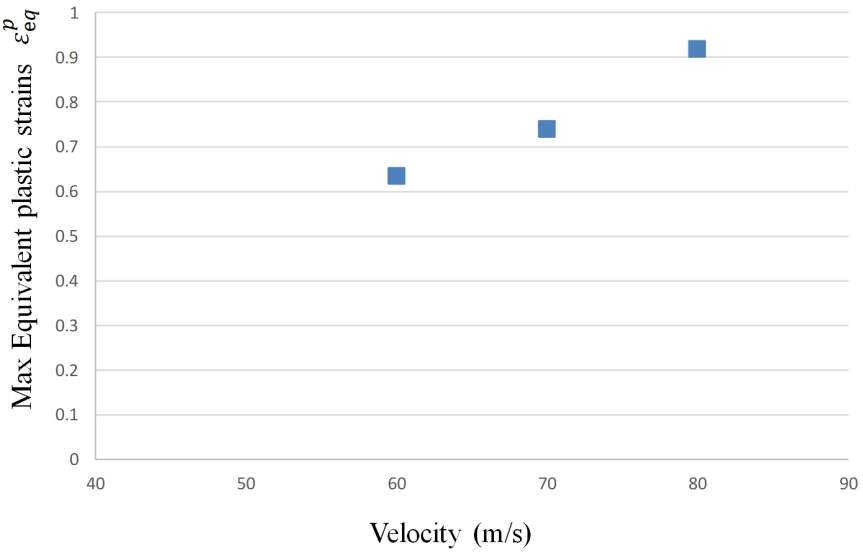

Figure 6.6: Maximum equivalent plastic strains vs. impact velocities.

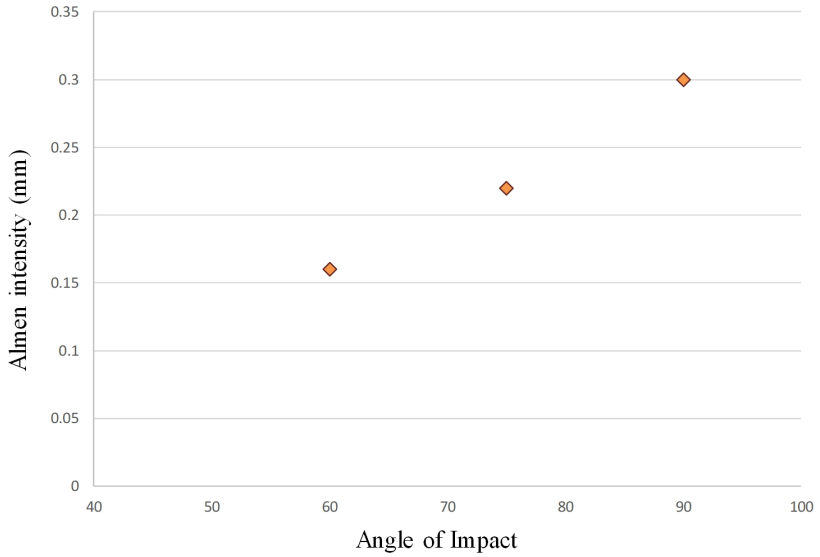

Figure 6.7: Effect of angle of impact on Almen intensity.

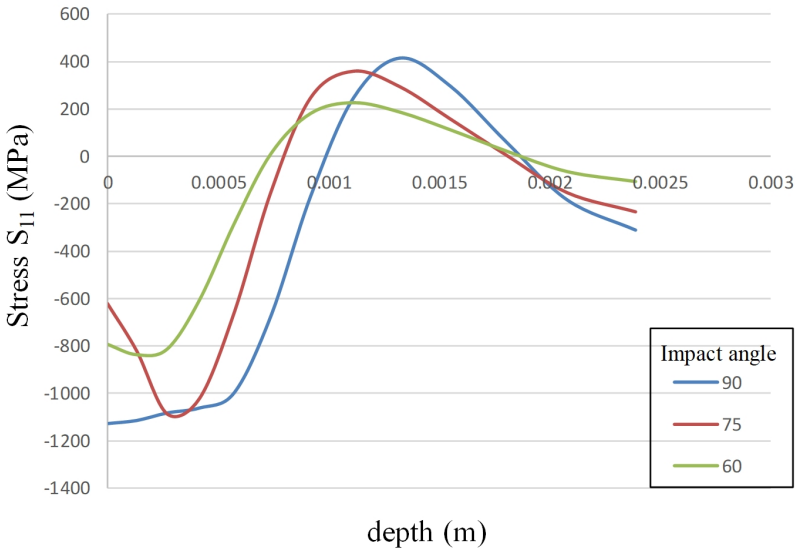

Figure 6.8: Effect of angle of impact on the induced stresses in constrained strip.

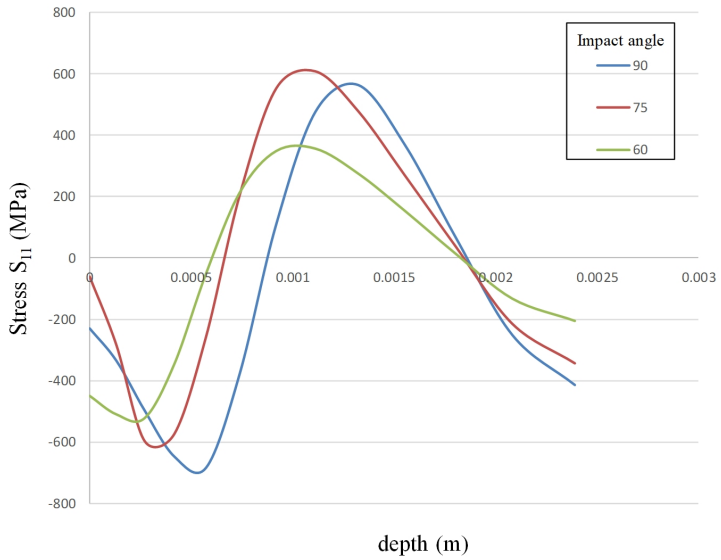

Figure 6.9: Effect of angle of impact on the residual stresses in unconstrained strip.

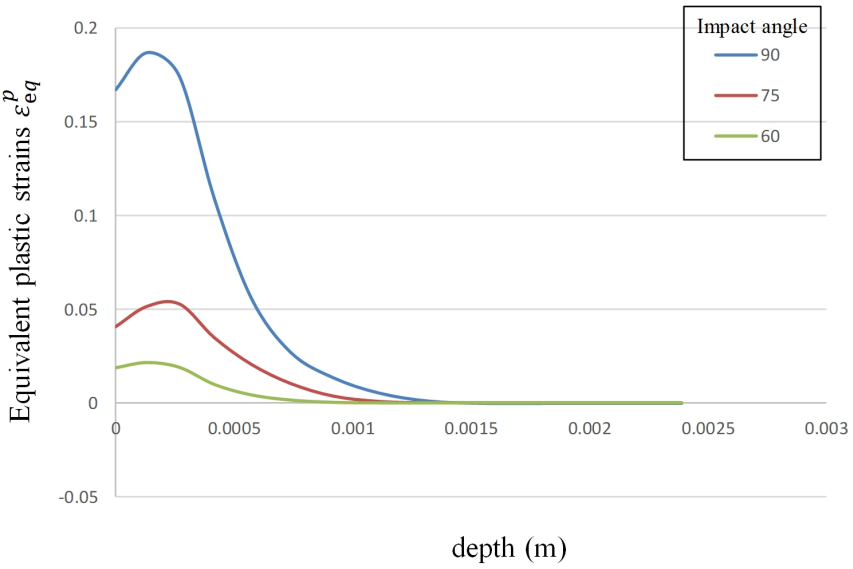

Figure 6.10: Effect of angle of impact on the equivalent plastic strains.

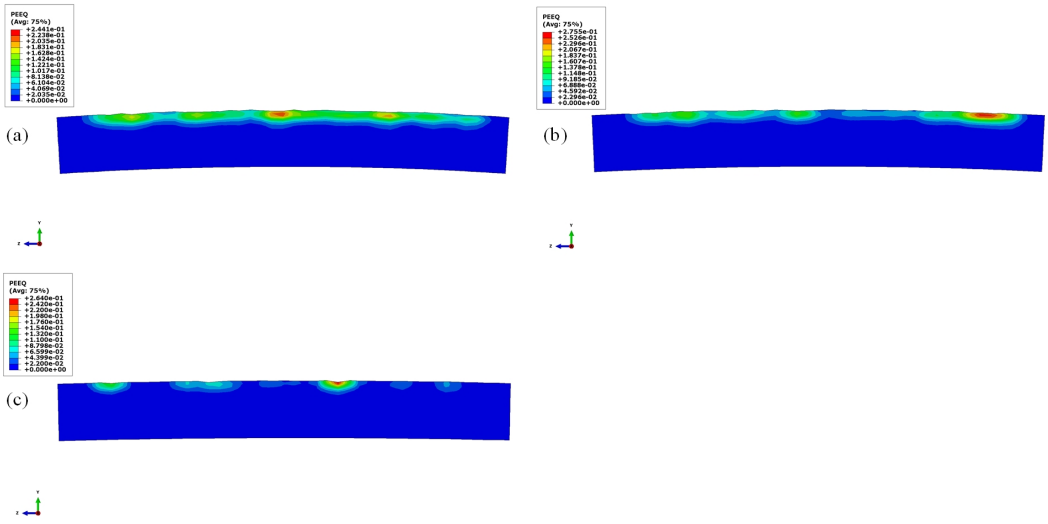

Figure 6.11: Equivalent plastic strains in a cross section vs impact angles (a) 90^o, (b) 75^o & (c) 60^o .

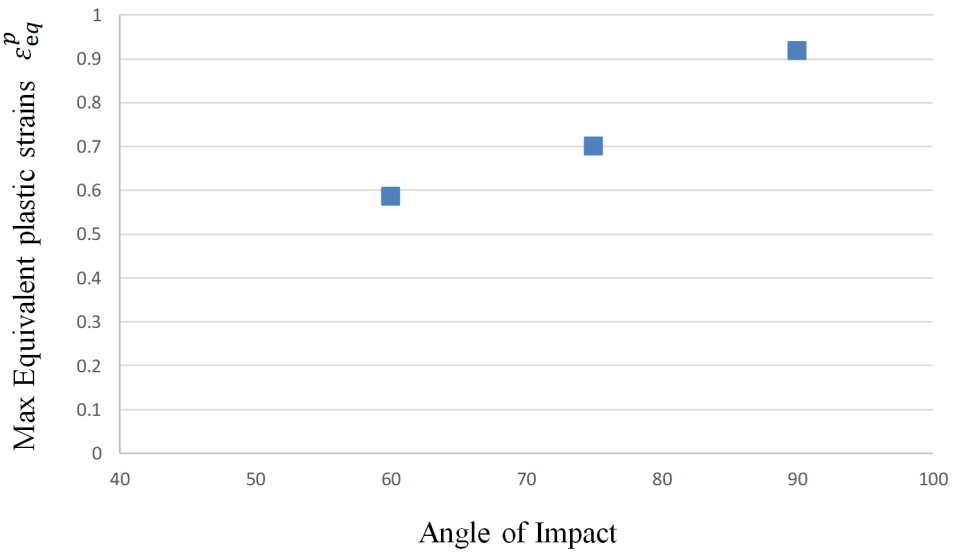

Figure 6.12: Maximum equivalent plastic strains vs. impact angles.

of impact decreases the depth of the induced compressive stresses also decreased. In the unconstrained state, the magnitude of the compressive residual stresses on the top surface decreased in magnitude compared to the constrained state. But the magnitude of the tensile residual stresses in the subsurface increased. And with the increase in the angle of impact, the magnitude of the compressive residual stresses in the bottom surface increased, as shown in figure 6.9.

Figure 6.10 shows the profile of the equivalent plastic strains along the thickness of the strip for different peening angles. As the angle of impact decreased, the magnitude of the equivalent plastic strains decreased significantly with a slight decrease in the depth of the plastic strains. Figure 6.11 shows the distribution of equivalent plastic strains in the cross-section of the Almen strip at its center for different impact angles. And the figure 6.12 shows the variation of maximum equivalent plastic strains in the Almen strip for different peening angles.

6.3 Shot size

Three different shot sizes (1 mm, 0.75 mm and 0.5 mm) are considered in this study. The shot speed is fixed at 80 m/s while the angle of impact is taken to be

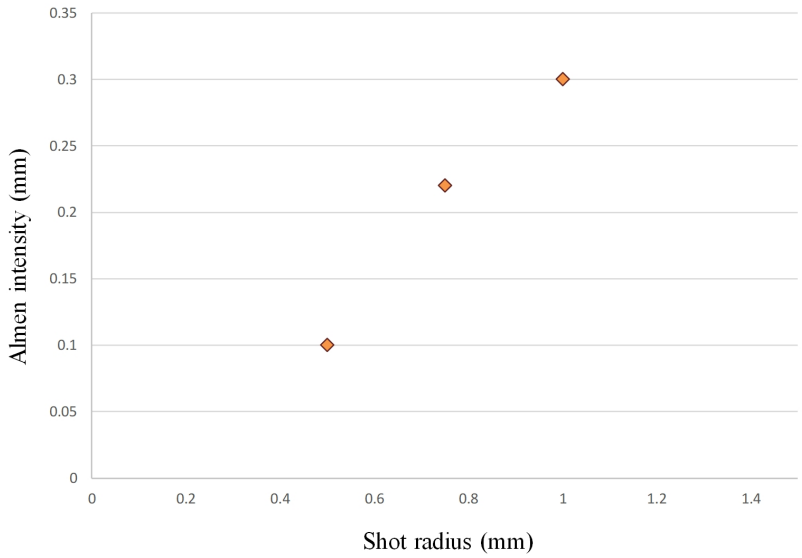

Figure 6.13: Effect of shot size on Almen intensity.

normal to the surface in all the three cases.

Figure 6.13 shows the effect of shot size on the Almen intensity. It is observed that with the decrease in the shot size there is a significant decrease in the intensity.

The variation of the induced stresses along the thickness of a constrained strip for different shot sizes is shown in figure 6.14. It is found that the magnitude of the induced stresses decreased significantly with the decrease in the shot radius. And also the stresses induced in the bottom surface are increasingly tensile with the decrease in shot size. In case of 0.5 mm shot radius, the stresses are tensile in the top surface with subsurface compressive stresses. Figure 6.15 shows the variation of the residual stress distribution in a free strip along its thickness for different shot sizes. It is found that the induced stresses in the top surface in case of larger shots relaxed more than that of the shots with a smaller radius.

Figure 6.16 shows the variation of the equivalent plastic stains along the thickness of the strip for different shot sizes. It is observed that as the shot size decreased the magnitude and depth of the equivalent plastic strains in the strip decreased significantly. Figure 6.17 shows the distribution of equivalent plastic strains in the cross-section of

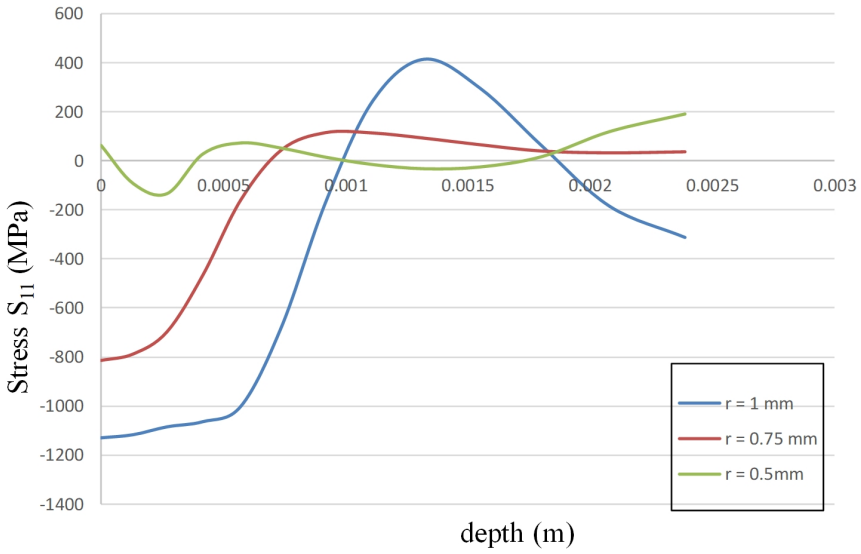

Figure 6.14: Effect of shot size on the induced stresses in constrained strip.

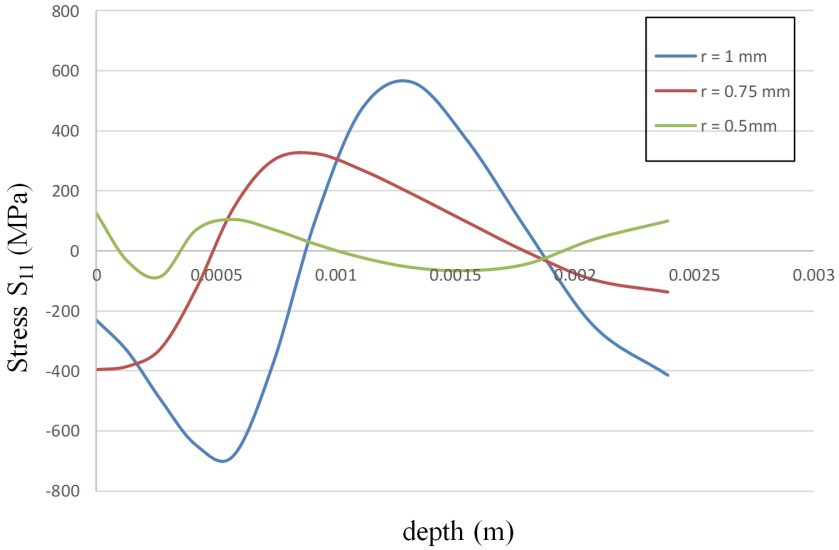

Figure 6.15: Effect of shot size on the residual stresses in unconstrained strip.

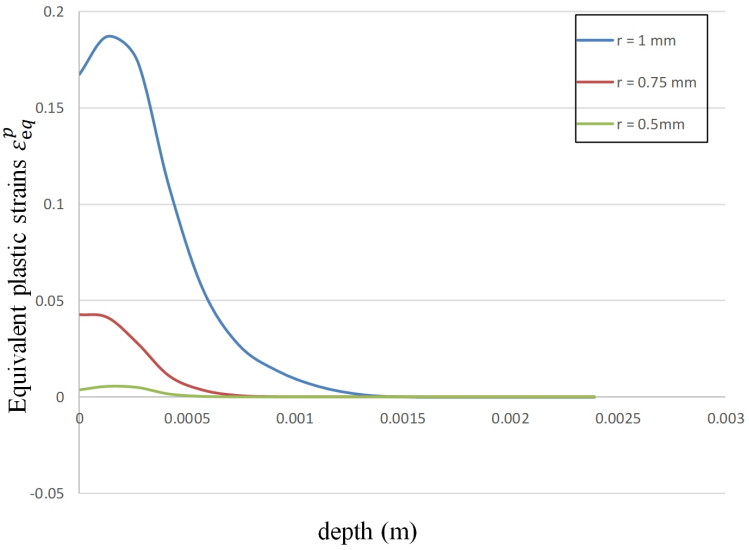

Figure 6.16: Effect of shot size on the equivalent plastic strains.

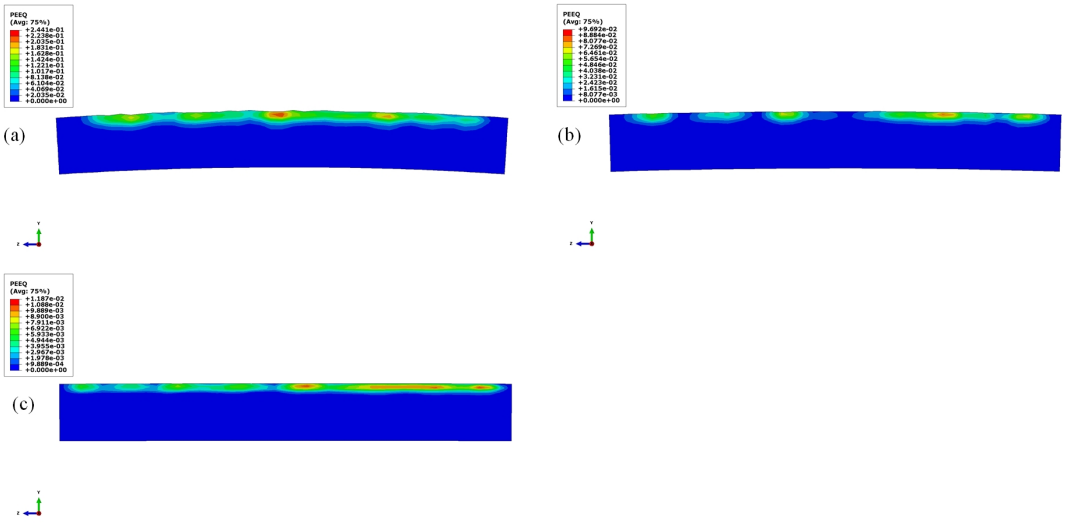

Figure 6.17: Equivalent plastic strains in a cross section vs shot size (a) 0.2 mm, (b) 0.15 mm & (c) 0.1 mm .

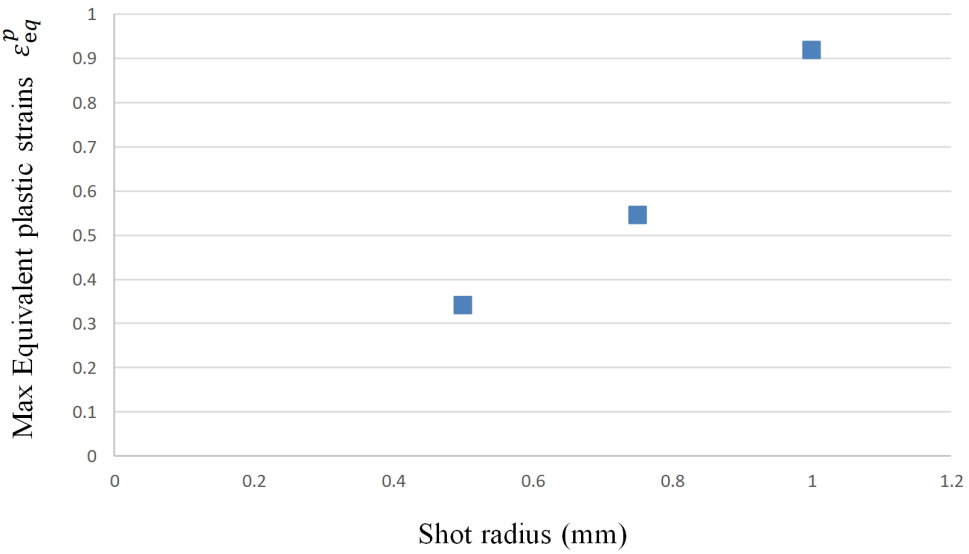

Figure 6.18: Maximum equivalent plastic strains vs. shot size.

the Almen strip at its center for different shot sizes. Figure 6.18 shows the variation of maximum equivalent plastic strains in the strip for different shot sizes, and it is observed that the magnitude of the maximum plastic strain decreased significantly with the decrease in shot size.

Table 6.1: Combinations of peening parameters for same Almen intensity.

Combination	Velocity (m/s)	Angle $(^o)$	Shot size (mm)
a	60	90	2
b	80	75	2
c	80	90	1.5

6.4 Almen intensity

In this study, it is observed that same Almen intensity can be obtained by using different combinations of peening parameters. Table 6.1 shows all the combinations of shot velocity, angle of impact and shot size for which the Almen intensity is found to be 0.22 mm. In Figure 6.19 and Figure 6.20 the stress profiles along the depth

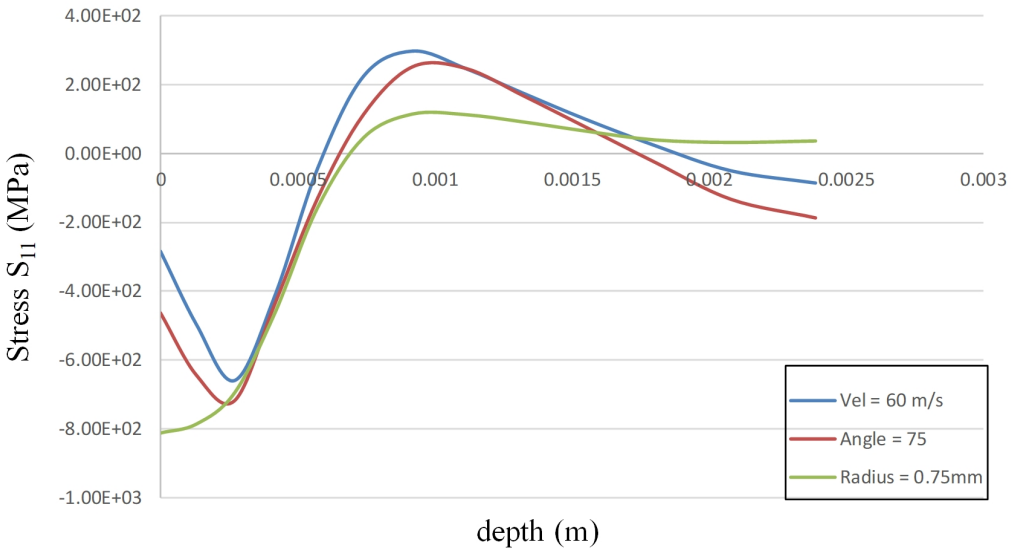

Figure 6.19: Induced stresses in a constrained strip.

of an Almen strip for different sets of peening parameters in both constrained and unconstrained states are shown respectively. It can be observed that for different sets of parameters even though the Almen intensities are same, the stress profiles vary from each other. Hence, it is important to select a proper set of parameters for shot peening at a certain intensity, as these parameters may effect the residual stress profiles in the components which in-turn effects their fatigue life. Figure 6.21 and Figure 6.22 shows the equivalent plastic strains in the strip along its depth and in a cross section respectively.

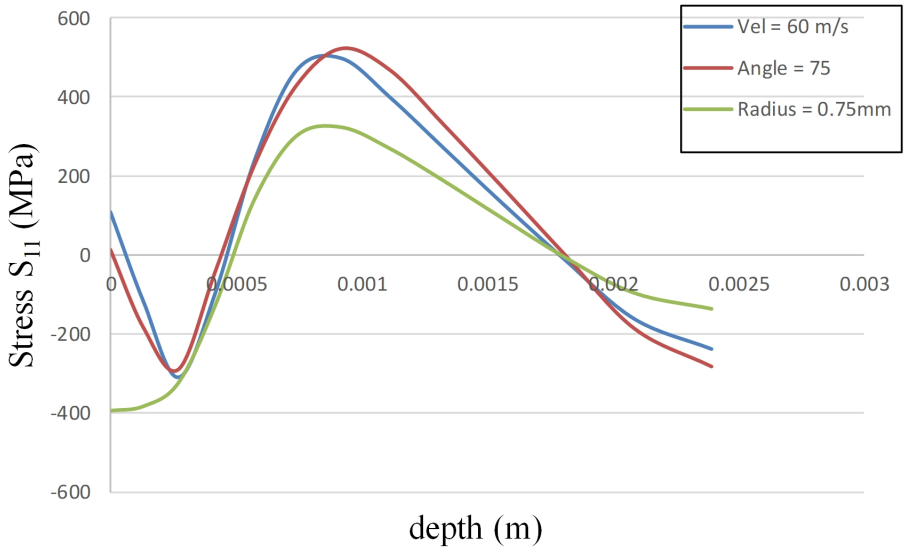

Figure 6.20: Residual stresses in an unconstrained strip.

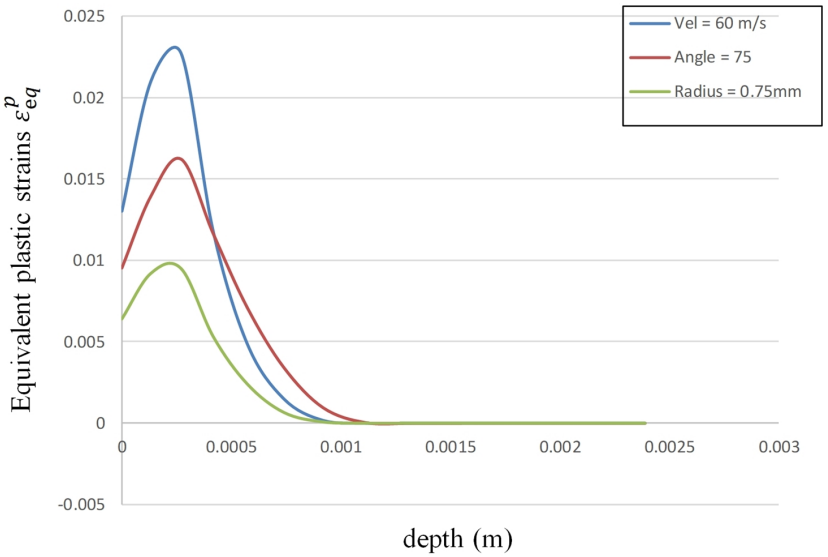

Figure 6.21: Equivalent plastic strains.

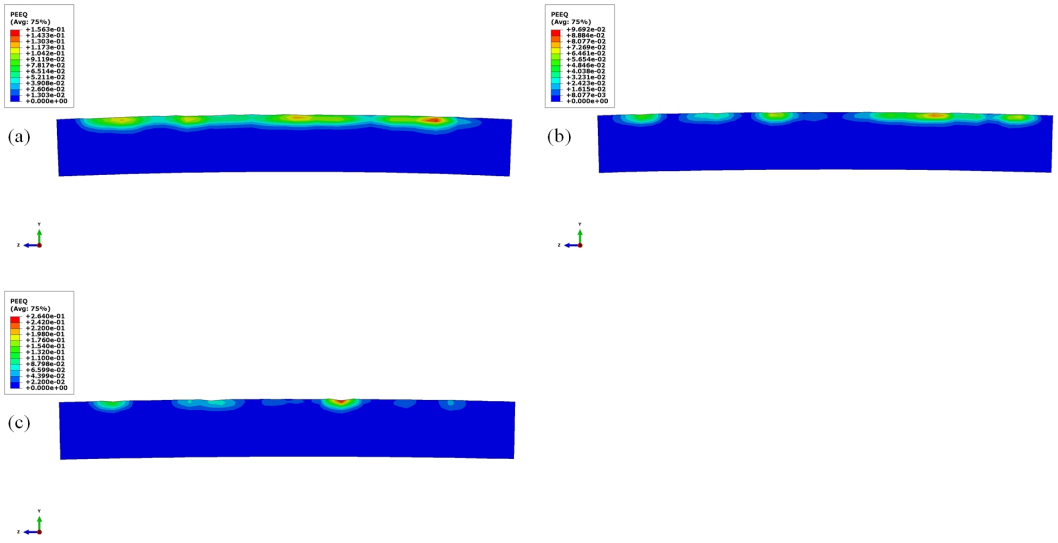

Figure 6.22: Equivalent plastic strains in a cross section (a) Velocity-70m/s, (b) Shot size-0.15mm & (c) Impact Angle-60^o .

CHAPTER 7: CONCLUSIONS

Almen intensity is one of the main shot peening control parameters to ensure the repeatability of the peening process. In this study, a numerical model is developed to predict the Almen intensity and to analyze the residual stress distribution in the Almen strip. A combination of discrete element method (DEM) and finite element method (FEM) is used to develop a full-scale model of the Almen intensity tests. The DEM capabilities of the finite element software package Abaqus\2017 are used to model the shot behavior. The influence of various shot peening parameters such as shot velocity, the angle of impact and shot size is presented.

Johnson-Cook constitutive model has been used to model the Almen strip to account for the strain rate effects during the shot peening process. The thermal softening term in the material model is neglected in this study. For the contact between the DEM particles and the Almen strip, a general contact algorithm is used in Abaqus. To simulate the shot peening process and the subsequent bending of the Almen strip a two-step analysis is used in Abaqus. To reduce the computational cost of the simulations, the results from one explicit analysis are transferred to the next to simulate the Almen strip tests for a different number of peening passes. The saturation curves for a different set of peening parameters are obtained by measuring and plotting the arc-heights against the peening passes. A two-parameter curve fitting tool [39] is used to calculate the Almen intensity. The simulated Almen intensities are compared with a published analytical model and found the results to be in good agreement.

The effect of springback analysis on the residual stress distribution is analyzed, and it is found that the stresses are predominantly compressive in the top surface and tensile in the bottom surface in the constrained strip. But when the constraints

are removed, to satisfy the equilibrium requirements, the stresses in the top surface become more tensile while the stresses in the bottom surface are compressive. Further, the variation of residual stresses and the equivalent plastic strains for a different number of peening passes are examined in both the constrained and unconstrained strips. The results reveal that the equivalent plastic strains are unaffected by the springback analysis while the residual stresses are readjusted to satisfy the self-equilibrating requirements. Also, the residual stresses and the plastic strains increased with increase in the number of passes.

Additionally, the variation of Almen intensities, equivalent plastic strains, induced and residual stresses in the Almen strip for different shot velocities, the angle of impact and shot size are analyzed. And based on the results, it is found that same Almen intensity can be obtained for a different set of peening parameters. But for the same Almen intensity, the residual stress profiles are different for different sets of parameters. Hence, care must be taken when choosing the process parameters for a required Almen intensity, as it may affect the residual stress profile and in-turn will affect the fatigue life of the peened components. Based on these results it can be concluded that the model proposed in this study can be used to simulate the shot peening process accurately and can be used to study the effect of various process parameters on the Almen intensities and the residual stress profiles in a full-sized Almen strip. Further, this model can be used to simulate the shot peening process on a full-size component to study the developed residual stress state.

In this study, to reduce the computational cost of the model, the shot-shot interactions are neglected, and high mass flow rates are used. But it should be noted that in a typical shot peening process, the shot-shot interactions influence the impacting velocity and in-turn will affect the induced stresses in the target. Further, the use of high mass flow rates can lead to increase in the shot-shot interactions. Hence in the future work, the shot-shot interactions can be incorporated into the model to study

the influence of mass flow rates, the distance of the nozzle from the workpiece and the nozzle dimensions on the quality of the shot peening process. The interactions between the shots can be easily incorporated in the present model by defining a contact pair in the general contact algorithm used in this study.

REFERENCES

[1] S. Maddox, "Influence of tensile residual stresses on the fatigue behavior of welded joints in steel," in *Residual Stress Effects in Fatigue*, ASTM International, 1982.

[2] G. Webster and A. Ezeilo, "Residual stress distributions and their influence on fatigue lifetimes," *International Journal of Fatigue*, vol. 23, pp. 375–383, 2001.

[3] C. Garcia, T. Lotz, M. Martinez, A. Artemev, R. Alderliesten, and R. Benedictus, "Fatigue crack growth in residual stress fields," *International Journal of Fatigue*, vol. 87, pp. 326–338, 2016.

[4] J. Davis, *Analytical modeling and applications of residual stresses induced by shot peening*. PhD thesis, University of Washington, 2012.

[5] J. Champaigne, "History of shot peening specifications," *Shot Peener*, vol. 20, no. 2, p. 12, 2006.

[6] M. Kobayashi, T. Matsui, and Y. Murakami, "Mechanism of creation of compressive residual stress by shot peening," *International Journal of Fatigue*, vol. 20, no. 5, pp. 351–357, 1998.

[7] J. O. Almen and P. H. Black, *Residual stresses and fatigue in metals*. McGraw-Hill, 1963.

[8] H. Miao, D. Demers, S. Larose, C. Perron, and M. Lévesque, "Experimental study of shot peening and stress peen forming," *Journal of Materials Processing Technology*, vol. 210, no. 15, pp. 2089–2102, 2010.

[9] B. Bhuvaraghan, S. M. Srinivasan, and B. Maffeo, "Numerical simulation of almen strip response due to random impacts with strain-rate effects," *International Journal of Mechanical Sciences*, vol. 53, no. 6, pp. 417–424, 2011.

[10] W. Cao, R. Fathallah, and L. Castex, "Correlation of almen arc height with residual stresses in shot peening process," *Materials science and technology*, vol. 11, no. 9, pp. 967–973, 1995.

[11] K. Johnson, "One hundred years of hertz contact," *Proceedings of the Institution of Mechanical Engineers*, vol. 196, no. 1, pp. 363–378, 1982.

[12] J. Li, Y. Mei, W. Duo, and W. Renzhi, "Mechanical approach to the residual stress field induced by shot peening," *Materials Science and Engineering: A*, vol. 147, no. 2, pp. 167–173, 1991.

[13] M. Guagliano, "Relating almen intensity to residual stresses induced by shot peening: a numerical approach," *Journal of Materials Processing Technology*, vol. 110, no. 3, pp. 277–286, 2001.

[14] H. Miao, S. Larose, C. Perron, and M. Lévesque, "An analytical approach to relate shot peening parameters to almen intensity," *Surface and Coatings Technology*, vol. 205, no. 7, pp. 2055–2066, 2010.

[15] H. Guechichi, L. Castex, and M. Benkhettab, "An analytical model to relate shot peening almen intensity to shot velocity," *Mechanics Based Design of Structures and Machines*, vol. 41, no. 1, pp. 79–99, 2013.

[16] V. Schulze, M. Zimmermann, and M. Klemenz, "State of the art in shot peening simulation," in *Proceedings of 10th International Conference on Shot Peening, Tokyo, Japan, September*, pp. 15–18, 2008.

[17] P. Follansbee and G. Sinclair, "Quasi-static normal indentation of an elasto-plastic half-space by a rigid sphereâi: Analysis," *International Journal of solids and structures*, vol. 20, no. 1, pp. 81–91, 1984.

[18] G. Sinclair, P. Follansbee, and K. Johnson, "Quasi-static normal indentation of an elasto-plastic half-space by a rigid sphereâii. results," *International Journal of solids and structures*, vol. 21, no. 8, pp. 865–888, 1985.

[19] K.-i. Mori, K. Osakada, and N. Matsuoka, "Rigid-plastic finite element simulation of peening process with plastically deforming shot," *JSME international journal. Ser. A, Mechanics and material engineering*, vol. 39, no. 3, pp. 306–312, 1996.

[20] K. Schiffner *et al.*, "Simulation of residual stresses by shot peening," *Computers & structures*, vol. 72, no. 1-3, pp. 329–340, 1999.

[21] T. Hong, J. Ooi, and B. Shaw, "A numerical study of the residual stress pattern from single shot impacting on a metallic component," *Advances in Engineering Software*, vol. 39, no. 9, pp. 743–756, 2008.

[22] Y. Al-Obaid, "Three-dimensional dynamic finite element analysis for shot-peening mechanics," *Computers & Structures*, vol. 36, no. 4, pp. 681–689, 1990.

[23] S. Meguid, G. Shagal, and J. Stranart, "Finite element modelling of shot-peening residual stresses," *Journal of Materials Processing Technology*, vol. 92, pp. 401–404, 1999.

[24] R. Shivpuri, X. Cheng, and Y. Mao, "Elasto-plastic pseudo-dynamic numerical model for the design of shot peening process parameters," *Materials & Design*, vol. 30, no. 8, pp. 3112–3120, 2009.

[25] S. Meguid, G. Shagal, and J. Stranart, "3d fe analysis of peening of strain-rate sensitive materials using multiple impingement model," *International Journal of Impact Engineering*, vol. 27, no. 2, pp. 119–134, 2002.

[26] G. Majzoobi, R. Azizi, and A. A. Nia, "A three-dimensional simulation of shot peening process using multiple shot impacts," *Journal of Materials Processing Technology*, vol. 164, pp. 1226–1234, 2005.

[27] H. Miao, S. Larose, C. Perron, and M. Lévesque, "On the potential applications of a 3d random finite element model for the simulation of shot peening," *Advances in Engineering Software*, vol. 40, no. 10, pp. 1023–1038, 2009.

[28] X. Kang, T. Wang, and J. Platts, "Multiple impact modelling for shot peening and peen forming," *Proceedings of the Institution of Mechanical Engineers, Part B: Journal of engineering manufacture*, vol. 224, no. 5, pp. 689–697, 2010.

[29] Z. Chen, F. Yang, and S. Meguid, "Realistic finite element simulations of arc-height development in shot-peened almen strips," *Journal of Engineering Materials and Technology*, vol. 136, no. 4, p. 041002, 2014.

[30] B. Bhuvaraghan, S. M. Srinivasan, B. Maffeo, R. D. McCLain, Y. Potdar, and O. Prakash, "Shot peening simulation using discrete and finite element methods," *Advances in Engineering Software*, vol. 41, no. 12, pp. 1266–1276, 2010.

[31] K. Murugaratnam, S. Utili, and N. Petrinic, "A combined dem–fem numerical method for shot peening parameter optimisation," *Advances in Engineering Software*, vol. 79, pp. 13–26, 2015.

[32] M. Jebahi, A. Gakwaya, J. Lévesque, O. Mechri, and K. Ba, "Robust methodology to simulate real shot peening process using discrete-continuum coupling method," *International Journal of Mechanical Sciences*, vol. 107, pp. 21–33, 2016.

[33] H. Zhu, Z. Zhou, R. Yang, and A. Yu, "Discrete particle simulation of particulate systems: theoretical developments," *Chemical Engineering Science*, vol. 62, no. 13, pp. 3378–3396, 2007.

[34] P. A. Cundall and O. D. Strack, "A discrete numerical model for granular assemblies," *geotechnique*, vol. 29, no. 1, pp. 47–65, 1979.

[35] C. O'Sullivan, *Particulate discrete element modelling: a geomechanics perspective*. Taylor & Francis, 2011.

[36] "Abaqus 2017 documentation." `https://help.3ds.com/2017/English/DSSIMULIA_Established`.

[37] K. Han, D. Peric, D. Owen, and J. Yu, "A combined finite/discrete element simulation of shot peening processes–part ii: 3d interaction laws," *Engineering Computations*, vol. 17, no. 6, pp. 680–702, 2000.

[38] R. VanLuchene, J. Johnson, and R. Carpenter, "Induced stress relationships for wing skin forming by shot peening," *Journal of materials engineering and performance*, vol. 4, no. 3, pp. 283–290, 1995.

[39] "Saturation curve solver." `https://www.shotpeener.com/tools/Solver_manual_msOffice2007.pdf`.